# Emissions of trace organic gases from western U.S. wildfires based on WE--CAN aircraft measurements

**Wade Permar[1], Qian Wang[1, 7], Vanessa Selimovic[1], Catherine Wielgasz[1], Robert J. Yokelson[1], Rebecca S. Hornbrook[2], Alan J. Hills[2], Eric C. Apel[2], I-Ting Ku[3], Yong Zhou[3], Barkley C. Sive[4], Amy P. Sullivan[3], Jeffrey L. Collett Jr[3], Teresa L. Campos[2], Brett B. Palm[5], Qiaoyun Peng[5], Joel A. Thornton[5], Lauren A. Garofalo[6], Delphine K. Farmer[6], Sonia M. Kreidenweis[6], Ezra J. T. Levin[3, 8], Paul J. DeMott[3], Frank Flocke[2], Emily V. Fischer[3], Lu Hu[1]**

[1]Department of Chemistry and Biochemistry, University of Montana, Missoula, MT, USA.

[2]Atmospheric Chemistry Observations & Modeling Laboratory, National Center for Atmospheric Research, Boulder, CO, USA.

[3]Department of Atmospheric Science, Colorado State University, Fort Collins, CO, USA.

[4]Air Resources Division, National Park Service, Denver, CO, USA.

[5]Department of Atmospheric Sciences, University of Washington, Seattle, WA, USA.

[6]Department of Chemistry, Colorado State University, Fort Collins, CO, USA.

[7]Now at Guizhou Provincial Key Laboratory of Geographic State Monitoring of Watershed, Guizhou Education University, Guiyang 550018, China.

[8]Now at Handix Scientific, Boulder, CO, USA.

Correspondence author: Lu Hu (lu.hu@mso.umt.edu)

**Key Points:**

- Volatile organic compound emission factors and emission ratios for western U.S. wildfires are reported.
- 76% of the total measured volatile organic compound emitted mass has statistically significant dependence on modified combustion efficiency.
- Mass fraction contributions of individual species to the total measured emissions have little fire-to-fire variability.

## Abstract

We present emissions measurements of volatile organic compounds (VOCs) for western U.S. wildland fires made on the NSF/NCAR C-130 research aircraft during the Western Wildfire Experiment for Cloud Chemistry, Aerosol Absorption, and Nitrogen (WE-CAN) field campaign in summer 2018. VOCs were measured with complementary instruments onboard the C-130, including a proton-transfer-reaction time-of-flight mass spectrometer (PTR-ToF-MS) and two gas chromatography (GC)-based methods. Agreement within combined instrument uncertainties (< 60 %) was observed for most co-measured VOCs. GC-based measurements speciated the isomeric contributions to selected PTR-ToF-MS ion masses and generally showed little fire-to-fire variation. We report emission ratios (ERs) and emission factors (EFs) for 161 VOCs measured in 31 near-fire smoke plume transects of 24 specific individual fires sampled in the afternoon when burning conditions are typically most active. Modified combustion efficiency (MCE) ranged from 0.85–0.94. The measured campaign-average total VOC EF was 26.1 ± 6.9 g $kg^{-1}$, approximately 67% of which is accounted for by oxygenated VOCs. The 10 most abundantly emitted species contributed more than half of the total measured VOC mass. We found that MCE alone explained nearly 70 % of the observed variance for total measured VOC emissions ($r^2$ = 0.67) and > 50 % for 57 individual VOC EFs representing more than half the organic carbon mass. Finally, we found little fire-to-fire variability for the mass fraction contributions of individual species to the total measured VOC emissions, suggesting that a single speciation profile can describe VOC emissions for the wildfires in coniferous ecosystems sampled during WE-CAN.


## 1 Introduction

Wildland fires are a significant source of non-methane volatile organic compounds (VOCs) to the atmosphere (Akagi et al., 2011; Crutzen & Andreae, 1991; Hatch et al., 2017; Koss et al., 2018; Liu et al., 2017), impacting downwind air quality, public health, and the formation of secondary pollutants such as ozone ($O_3$), and secondary organic aerosol (SOA). However, their global and regional emissions are highly uncertain, in part reflecting the scarcity of field measurements to constrain VOC emissions from biomass burning. As the size and intensity of wildfires have increased due to historic forest management practices and climate change (Bowman et al., 2017; Jolly, 2015; Westerling, 2006, 2016), air quality in the western United States (U.S.) is degrading relative to the rest of the country (McClure & Jaffe, 2018; O'Dell et al., 2019). These issues motivated comprehensive smoke characterization measurements from the National Science Foundation / National Center for Atmospheric Research (NSF/NCAR) C-130 research aircraft for western U.S. wildfires during the 2018 Western Wildfire Experiment for Cloud Chemistry, Aerosol Absorption, and Nitrogen (WE-CAN) field campaign.

Biomass burning emission factors (EFs, g compound emitted per kg biomass burned) are a critical input to air quality models which rely mainly on "bottom-up" emissions inventories derived from regional or vegetation specific EFs, burned area, and fuel consumption per unit area (Larkin et al., 2014; Urbanski, 2014; van der Werf et al., 2017; Wiedinmyer et al., 2011). Total emissions are subject to large uncertainties given the difficulty of estimating burned area and fuel consumption along with large fire-to-fire VOC emissions variability and a general under-sampling of many wildfire-prone regions, including the western U.S. The large natural fire-to-fire variability of some commonly measured VOC emissions can be partially explained by a simple proxy of "flaming" and "smoldering" combustion processes, known as the modified combustion efficiency (MCE), which is readily calculated from observations of carbon monoxide (CO) and carbon dioxide ($CO_2$) (Akagi et al., 2013; Andreae & Merlet, 2001; Ferek et al., 1998; Guérette et al., 2018; Liu et al., 2017; Urbanski, 2014; Yokelson et al., 1999).

To better constrain VOC and other air pollutant emissions from western U.S. fires, several recent large laboratory burn experimental studies have been conducted for representative fuels (Gilman et al., 2015; Hatch et al., 2017; Koss et al., 2018; Selimovic et al., 2018; Stockwell et al., 2014, 2015; Yokelson et al., 2013). Laboratory experiments attempt to simulate real-world burning conditions using fuels selected to reflect their natural composition, sometimes resulting in good agreement between field and laboratory measured EFs and emission ratios (ERs) of well-characterized species (Akagi et al., 2013; Christian et al., 2003; Selimovic et al., 2018; Yokelson et al., 2008, 2013). However, laboratory burning experiments are imperfect proxies for the complexity of the dynamic burning processes, meteorological conditions, and varying fuels present in wildland fires. Meanwhile, field emission measurements, either using ground- or airborne-based platforms, are typically limited by how near a wildfire they can sample due to safety and logistical constraints. As chemical processes take place in the smoke plume within tens of minutes between emission and sampling by research aircraft (Hobbs et al., 2003; Peng et al., 2020), field emission measurements likely reflect some removal of highly reactive species along with formation of secondary products. Airborne measurements may also miss emissions from residual smoldering combustion (Bertschi et al., 2003), which tend to not be lofted into the main convective column of the plume, while ground based measurements reflect the opposite problem as they are often unable to sample portions of the smoke most impacted by flaming

emissions (Akagi et al., 2013; Ottmar, 2014; Prichard et al., 2020; Yokelson et al., 2013). Additionally, laboratory studies can allow for a large suite of analytical instrumentation to sample smoke within meters of a fire, from ignition to extinction. Field measurements are often limited by instrument payload and these samples include emissions from a variety of burning conditions. Consequently, to most accurately characterize wildfire emissions, insights gained from laboratory studies are useful in the interpretation of field measurements (Selimovic et al., 2019).

Hundreds, if not thousands, of VOCs are known to be present in biomass burning smoke (Bruns et al., 2017; Hatch et al., 2017; Koss et al., 2018; Müller et al., 2016; Stockwell et al., 2015). Characterization of these VOCs remains a challenge though as no single technique is best suited to measure such a large variety of compounds, particularly at the temporal resolution needed for aircraft sampling. Chemical ionization mass spectrometry (CIMS), such as proton-transfer-reaction time-of-flight mass spectrometry (PTR-ToF-MS), is capable of measuring hundreds of VOCs at < 1 s, but lacks speciation information without prior knowledge of the sampling medium. Gas chromatography (GC)-based systems are highly complementary to CIMS instruments, providing speciated VOC measurements with low ppt detection limits at lower temporal resolution. During the recent Fire Influence on Regional to Global Environments Missoula Fire Lab experiment (FIREX-MFL), https://www.esrl.noaa.gov/csl/projects/firex/firelab), Koss et al. (2018) identified the VOC contributors to more than 150 ions detected by PTR-ToF-MS (~90 % of the total detected VOC mass) through a combination of approaches including gas chromatography pre-separation, two chemical ionization methods, literature review, and time series correlation. Additionally, Sekimoto et al. (2017) showed that sensitives for many VOCs without direct calibrations in PTR-ToF-MS can be calculated to within 50 % using readily available molecular properties such as polarizability, dipole moment, and functionality.

In this work, we utilize data from the co-deployed GC-based Trace Organic Gas Analyzer (TOGA) and the Advanced Whole Air Sampler (AWAS), while building extensively off previous identification, calibration, and validation efforts for PTR-ToF-MS, to report

comprehensive VOC emissions for western U.S. wildfires. The unprecedented large number of wildfires sampled during WE-CAN allows us to explore the variability of VOCs that are emitted and how they are related to combustion processes.

## 2 Methods

### 2.1 WE-CAN field campaign

The WE-CAN field campaign was based in Boise, ID, from 24 July to 31 August and Broomfield, CO from 1 September to 13 September 2018 (https://www.eol.ucar.edu/field_projects/we-can). Nineteen flights were conducted by the NSF/NCAR C-130 research aircraft approximately every 1–3 days and sampled smoke from > 20 fires across seven western states. Smoke plumes were typically sampled between 14:00 and 19:00 local time when burning conditions were most active. Most sampled smoke plumes were emanating from wildfires located in mixed coniferous forests with burned fuels consisting primarily of pine, fir, and spruce trees (http://catalog.eol.ucar.edu/we-can/tools/fccs). Sampling was done by flying perpendicular transects through each smoke plume as near to the source as was allowed by safety and logistical constraints. Emissions were assessed using transects that proceeded as follows. The C-130 entered into each plume after sampling background air as determined by real-time CO observations in flight and continued through the plume until the CO mixing ratios reached regional background levels (generally 75–175 ppb), ideally similar to the mixing ratios observed prior to entering the plume. During WE-CAN, the C-130 also sampled smoke plumes in a pseudo-Lagrangian fashion to characterize smoke evolution (Akagi et al., 2012); other portions of the flights were devoted to sampling cloud-smoke mixtures and aged regional smoke plumes in specific locations.

### 2.2 Proton-transfer-reaction time-of-flight mass spectrometer

We deployed the University of Montana proton-transfer-reaction time-of-flight mass spectrometer (PTR-ToF-MS 4000, Ionicon Analytik, Innsbruck, Austria) aboard the NSF/NCAR C-130 during WE-CAN. The PTR-ToF-MS is custom-built into a standard NSF/NCAR HIAPER Gulfstream-V (GV) rack with the mass spectrometer separately vibration dampened. Drift tube conditions were maintained at 3.00 mbar, 810 V, and 60 °C, resulting in E/N of 130 Td for the duration of the campaign. Ion *m/z* from 15–400 were measured at 2 or 5 Hz frequency with a

mass resolution of 2250 $m/\Delta m$ at $m/z$ 33.033 to 4000 $m/\Delta m$ at $m/z$ 330.842, where $\Delta m$ is the full width at half mass for an ion peak of mass $m$.

The PTR-ToF-MS inlet was positioned below the instrument rack, mid-cabin underneath the aircraft. Ambient air was drawn into the cabin at 10–15 lpm, dependent on altitude, via a heated (60 °C) NCAR HIAPER Modular Inlet (HIMIL) attached to a downstream pump (KNF Neuberger Inc., Trenton, NJ). From the HIMIL to the instrument rack, sampled air traveled a distance of ~3 m through a 3.175 mm I.D. PFA tubing maintained at ~55 °C by a self-regulating heat cable. At the rack, the sample stream was subsampled by the PTR-ToF-MS through ~100 cm of 1.588 mm O.D. PEEK tubing maintained at 60 °C. The residence time from outside the plane to the drift tube was less than 2 seconds. A detailed schematic of our instrument inlet and sampling setup is provided in Figure S1.

For a typical research flight, the PTR-ToF-MS was powered on and allowed to pump down starting 3 hours prior to take-off. Instrument background was checked approximately every hour by measuring VOC-free air generated from a heated catalytic converter (375 °C, platinum bead, 1 % wt. Pt, Sigma Aldrich) for 3 minutes. Real-time mass calibrations were performed every 5 seconds using an internal 1,3-diiodobenzene ($C_6H_4I_2$) reference standard added directly to the drift tube from an adjacent heated permeation device.

Mass spectra were analyzed using Ionicon's PTR-MS Viewer software (version 3.2.8.0, Ionicon Analytik, Innsbruck, Austria). Post flight mass calibrations were done to further refine the real-time mass calibration using 5 ion peaks: $m/z$ 18.0338 [$NH_3H^+$], 29.9971 [$NO^+$], 59.0491 [$C_3H_6OH^+$], 203.943 [$C_6H_4IH^+$], and 330.848 [$C_6H_4I_2H^+$]. Chemical formula for each ion mass were assigned using a peak list native to the software as well as derived from the growing PTR-ToF-MS literature (Koss et al., 2018; Pagonis et al., 2019). A high-resolution peak fitting algorithm was then manually adjusted for individual peak shapes and PTR-MS Viewer calculated ion counts for each peak, performing a baseline correction, and correcting for mass

discrimination in the time-of-flight following common standard PTR-ToF-MS data analysis procedures (Yuan et al., 2017).

Mass transmission corrected raw instrument signals were exported for post-processing in R (R Core Team, 2019), using the open source software RStudio with the dplyr and ggplot2 packages (RStudio Team, 2020; Wickham, 2016; Wickham et al., 2019). Ion masses were first background corrected by subtracting the linearly interpolated instrument background measured in-flight. Ion counts were then normalized to the primary ion signal and a humidity correction factor was applied for those VOCs which were calibrated by the gas standard (de Gouw et al., 2003). PTR-ToF-MS data in normalized counts per second (ncps) were averaged to 1 Hz and converted to mixing ratios as described in Section 2.2.2 for all subsequent analyses.

#### 2.2.1 Identification and speciation of PTR-ToF-MS ion masses

Overlapping speciated VOC measurements available on the C-130 during WE-CAN (Section 3) allow us to identify and assign isomeric fractional contributions to four PTR-ToF-MS ions masses (Table S1): *m/*z 59.049, *m/*z 71.049, *m/*z 107.086, and *m/*z 137.132. For the remaining ions, we applied available isomeric contributions measured during the FIREX-MFL study, which burned similar western U.S. fuel types and speciated PTR-ToF-MS ion peaks for an instrument with similar mass resolving power to the one deployed during WE-CAN (Koss et al., 2018). Although the actual isomeric contributions may differ, especially for relatively reactive species, the consistent treatment of PTR-ToF-MS measurements between FIREX-MFL and WE-CAN allows for more direct comparison of the emission factors determined in the laboratory to our field observations (Section 6). The overall measurement uncertainty caused by assumptions in isomeric contributions are mostly governed by the instrument sensitivities for all isomers which differ by less than 50 % at any given ion mass, indicating that the impact on mixing ratio is within the error of the calculated sensitivities (see Section 2.2.2)

During WE-CAN, we quantified 125 of 154 identified ions (excluding ammonia, $NH_3$, and nitrous acid, HONO) reported during FIREX-MFL (Koss et al., 2018). The remaining 29 ions accounted for less than 2 % of the FIREX-MFL PTR-ToF-MS total measured VOC mass (sum

of VOC EFs). Additional quantification in the laboratory resulted largely from Fourier-transform infrared spectroscopy (FTIR) co-measured data for $NH_3$ and HONO and the fact that laboratory burning experiments measure emissions at ~10 times higher sample concentrations than field observations (e.g., Figure 2, Stockwell et al., 2014). In later sections, we discuss if the identification and speciation of ion masses from laboratory studies are represented in the field as constrained by the limited co-measured VOCs onboard the C-130 aircraft (Section 3), and describe how the difference of plume aging between laboratory and field measurements may affect emission factors (Section 6).

#### 2.2.2 Calibration

For each flight, we calibrated the instrument 3 times: 10 minutes before take-off, in-flight when in transit to/from a fire, and immediately after landing. Instrument calibrations were carried out by the dynamic dilution and subsequent addition of 25 distinct VOCs from two compressed gas standard cylinders (stated accuracy 5 % at ~1 ppmv; Apel-Riemer Environmental Inc., Miami, FL; species listed in Figure S2) to the VOC-free air described above. The standard gas cylinders were filled in June 2017 and were re-analyzed for selected VOCs before and after the WE-CAN campaign with the permeation device described below. Calibrations were carried out in the range of 1–10 ppb. Typical $r^2$ values for the 4-point calibration curve of all species were greater than 0.99 with average residual standard errors less than 10 % (in almost all cases < 3 %). The standard error (95 % confidence interval) of sensitivities for all calibrated VOCs was found to be < 9 % during WE-CAN, thus the campaign averaged sensitivities were applied to all flights. The overall uncertainty for gas standard calibrated species is < 15 %, which is based on the quadrature addition of the individual errors including mass flow controllers, standard accuracy, peak fitting, and calibration.

Additionally, we calibrated formaldehyde (HCHO) post WE-CAN using a gas standard (accuracy 5 % at 420 ppbv reanalyzed by FTIR in October 2019). We quantified the humidity dependent sensitivity by varying the water vapor in the zero air to the range observed during WE-CAN (i.e., [*m/z* 39]/[*m/z* 21], an internal humidity proxy, spanning 0–2 %) (Vlasenko et al., 2010; Warneke et al., 2011), and accounted for a possible sensitivity drift since WE-CAN based

on other gas standard calibrations. The formaldehyde measurement uncertainty is estimated to be 40 %, mostly contributed by instrument sensitivity drift since WE-CAN.

We also calibrated acetic acid ($CH_3COOH$) and formic acid (HCOOH) before and after the campaign using a custom built permeation system (Baasandorj et al., 2015; Haase et al., 2012; Veres et al., 2010). Here, a constant flow of 20 sccm of ultrapure zero air was passed over a PFA permeation tube (fabricated in-house), which was maintained at a constant temperature. The VOC mixing ratio from the permeation source was stoichiometrically determined by converting to $CO_2$ via passing through a heated catalyst (400 °C, platinum bead, 1 % wt. Pt, Sigma Aldrich) and subsequently measuring enhancement by a $CO_2$ detector (LI-840A, LI-COR Inc, Lincoln, NE). Analytes were then added into the PTR-ToF-MS via the above dynamic dilution calibration. The performance of the permeation system was verified by both certified permeation tubes and the multi-component gas standards. The uncertainty in the permeation calibrations is generally less than 30 %, contributed mostly by the LI-COR.

For the remaining ~180 identified VOC contributors that are not directly calibrated for, we estimated their instrument sensitivities using the method developed by Sekimoto et al. (2017). Briefly, molecular dipole moments and polarizability for each species are used to calculate a proton capture coefficient, $k_{cap}$, for the reaction with $H_3O^+$. $k_{cap}$ was shown to be linearly correlated to sensitivity for most VOCs:

$$Sensitivity_{calculated,i} = a \times k_{cap,i} \quad (1)$$

where the coefficient $a$ is experimentally determined from calibrated VOCs and their $k_{cap}$ ($a$ = 5.00 x $10^9$ for the instrument setting in WE-CAN). Chemical properties used here, including functional groups, polarizabilities, and dipole moments, are from the compiled PTR-ToF-MS Library (www.tinyurl.com/PTRLibrary; Pagonis et al., 2019).

The overall uncertainty for this method is estimated to be 50 % for most species and may be higher for select groups of VOCs (Sekimoto et al., 2017). The calculated and measured sensitivity for 26 directly calibrated VOCs are compared in Figure S2, showing agreement within the stated uncertainty. Sensitivity estimates are further verified for co-measured VOCs onboard the C-130 in Section 4.

Average sensitivities for each ion mass were subsequently determined using the weighted sensitivity of the known isomers following:

$$sensitivity_{average} = \left(\sum \frac{contribution_i}{sensitivity_i}\right)^{-1} \quad (2)$$

where $contribution_i$ is the isomeric contribution of VOC isomers to an ion mass (Section 2.2.1) and $sensitivity_i$ is the corresponding instrument calibration factor either from direct calibrations using gas standards or calculated using molecular properties. The overall uncertainty is then estimated by adding in quadrature errors from involved sensitivities weighted by isomeric contributions. Table S1 lists the sensitivities for 180 VOCs, along with their uncertainties, isomeric contributions to each mass, and calibration methods.

### 2.3 TOGA, AWAS, $I^-$ CIMS, and other supporting instrumentation

In addition to PTR-ToF-MS, we report VOCs measured by the Trace Organic Gas Analyzer (TOGA) (Apel et al., 2003, 2010, 2015; Hornbrook et al., 2011), Advanced Whole Air Sampler (AWAS) (Andrews et al., 2016), and iodide ($I^-$) adduct high-resolution time-of-flight chemical-ionization mass spectrometer ($I^-$ CIMS) (Lee et al., 2014; Palm et al., 2019; Peng et al., 2020). The TOGA and AWAS measurements greatly extend the emission analysis here to include many species not detected by PTR-ToF-MS, while also add isomer contributions for several ion masses. During WE-CAN, TOGA sampled ambient air for 28–33 seconds to a liquid nitrogen cooled cryogenic preconcentrator which was then analyzed for 72 VOCs every 100–105 seconds via a gas chromatography-mass spectrometer (GC-MS). The collection of AWAS canisters samples was manually initiated based on inflight measured CO mixing ratios targeting both

edges and the center of a plume. Typically, 1–3 canister samples were collected per emission transect in addition to background samples collected either just outside a smoke plume or behind the fire. Each canister was filled for 3–7 s and analyzed for 58 individual VOCs ($C_1$-$C_{10}$ hydrocarbons, $C_1$-$C_5$ alkyl nitrates, and oxygenated VOCs) using a five-channel gas chromatography system equipped with three flame ionization detectors, one electron capture detector and one mass spectrometer (Benedict et al., 2019, 2020; Russo et al., 2010; Zhou et al., 2010). Measurement uncertainties for TOGA and AWAS vary by compound but are typically between 15 and 50 % (TOGA) and < 10 % (AWAS). We also report HCOOH measured by $I^-$ CIMS because of its high sensitivity. $I^-$ CIMS HCOOH calibration uncertainty is 30 % and was measured at 2 Hz (Palm et al., 2019; Peng et al., 2020).

CO, measured at 1 Hz (accuracy 1 ppb, 2σ) by quantum cascade laser spectrometry (CS-108 miniQCL, Aerodyne Inc., Billerica, MA) was used for all analyses except for fires sampled on 13 August 2018 (RF10), where we used a cavity ring down spectrometer (G2401-m WS-CRD, Picarro, Santa Clara, CA) which also measured $CO_2$ (accuracy 100 ppb, 2σ) and $CH_4$ (accuracy 3 ppb, 2σ) at 1.3 Hz for the duration of the campaign.

Black carbon was measured by a single particle soot photometer (SP2) (Liu et al., 2017; Schwarz et al., 2008) and averaged to a 10 s sampling frequency. When in plume, the SP2 sample was diluted with HEPA-filtered ambient air to prevent signal saturation and has an uncertainty of 40 % when in the dilution system (Garofalo et al., 2019). Organic carbon (OC) was derived from the organic aerosol (OA) to OC ratio (OA:OC) measured by high-resolution aerosol mass spectrometry (HR-AMS; Aerodyne Inc., Billerica, MA) (Garofalo et al., 2019). For this, OC was calculated at each HR-AMS time stamp using the measured OA:OC. When the measured OA:OC was unavailable (ex., when OA is below the instrument detection limit), we used the calculated WE-CAN emission average OA:OC of 1.73. HR-AMS measurements were carried out at 5 s and have an uncertainty of 35 %.

328 2.4 Co-measured VOCs and data reduction

329 Of the 161 VOC species reported in this work, 34 were co-measured PTR-ToF-MS, TOGA
330 and/or AWAS. For overlapping VOC measurements, we used similar criteria as in Yokelson et
331 al. (2013) to determine which measurement to report. Selection criteria are hierarchically
332 described below.

333

334 1) Species that PTR-ToF-MS is known to have difficulty measuring because of low
335 sensitivities or interfering fragments were removed from the analysis and the appropriate
336 TOGA or AWAS measurement was used instead. These include hydrogen cyanide
337 (HCN), ethane ($C_2H_6$), ethanol ($C_2H_5OH$), and dimethyl sulfide (DMS, $(CH_3)_2S$).
338 Similarly, we removed PTR-ToF-MS measured isoprene ($C_5H_8$) due to possible fragment
339 interference as discussed in Section 4.

340

341 2) When selecting between species co-measured by TOGA and AWAS, we retained the
342 measurement reporting the most isomers for a giving chemical formula. When the
343 number of observed isomers was equal, we report the measurement with the greater
344 campaign average ER for that chemical formula in order to account for potential
345 unidentified species.

346

347 3) VOCs directly calibrated by the PTR-ToF-MS (Figure S2) were selected over TOGA or
348 AWAS measurements to preserve the high time resolution of the measurement. It also
349 helps minimize possible errors from (1) background correcting discrete samples, (2)
350 misalignment of the discrete data to the high-frequency CO measurements, and (3) the
351 potential for integrated samples only capturing part of a plume. For VOCs with known
352 isomers or fragments in PTR-ToF-MS, we also report the TOGA or AWAS measurement
353 as described in criteria 2. However, to prevent double counting, additional speciated
354 information was not used in EF mass balance or total emitted VOC calculations.

355

For example, PTR-ToF-MS measures the total of methyl vinyl ketone (MVK), methacrolein (MACR), and 2-butenal at *m/z* 71.049 ($C_4H_6OH^+$; Table S1). TOGA and AWAS both report individual MVK and MACR, with TOGA also measuring 2-butenal. For the EF calculations here, we used the PTR-ToF-MS measurement for *m/z* 71.049. Additionally, we report the TOGA MVK, MACR, and 2-butenal measurements in Table 2 to provide more detailed speciation, and because TOGA observed more isomers than AWAS. When totaling EFs or ERs, only the PTR-ToF-MS measurement was used.

4) For VOCs with calculated sensitivities, we used the PTR-ToF-MS measurement when campaign-average emission transect mixing ratios agree within 50 % of the sum TOGA or AWAS isomers for that mass. Additionally, if the PTR-ToF-MS does not agree within 50 % but there are known isomers not reported by TOGA or AWAS, we again report the PTR-ToF-MS measurement with TOGA or AWAS speciation as described in criteria 3. For the remaining species where the PTR-ToF-MS does not agree within 50 %, we again report the appropriate TOGA or AWAS measurement following criteria 2.

2.5 Calculations of emission factor, emission ratio, and modified combustion efficiency

We calculated WE-CAN EFs and ERs for 31 emission transects of 13 wildfires and 1 prescribed burn. Plume transects were chosen for inclusion based on the criteria of being from well-defined smoke plumes traceable to a single emission source, being the nearest transects to said source, and having physical age less than 130 minutes as calculated by wind speeds measured aboard the C-130 and fire locations reported by the U.S. Forest Service (http://catalog.eol.ucar.edu/we-can/tools/fuels). The latter criterion was chosen to reflect aging times in similar studies (Liu et al., 2017) and maximize the number of plume transects available to improve statistics. Recent studies have shown that rapid chemistry occurs within minutes after emission (Hobbs et al., 2003; Peng et al., 2020); later we discuss how this may affect the emission factors for some very reactive VOCs that we report here. For repeated sampling, we aggregate those plume transects which were performed in succession for the same fire within 30 minutes and treat those that are more than 30 minutes apart as ‘unique fires’. This results in 24 fires used in the emission analysis here (denoted a, b, c, etc.; Table 1 and Table S4).

386 **Table 1.** *Details of Fires Sampled During the WE-CAN Field Campaign Used in this Work.*

| Fire name[a] | Date (2018) | Flight | State | Num. passes[b] | Latitude | Longitude | Distance sampled downwind (km) | Physical age (minutes) | Burned area (ha)[c] |
|---|---|---|---|---|---|---|---|---|---|
| Carr (a, b) | July 26 | RF02 | CA | 1, 1 | 40.63° | -122.52° | 32.8–33.6 | 64–106 | 92,939 |
| Taylor Creek | July 30 | RF03 | OR | 2 | 42.47° | -123.69° | 11.5–13.7 | 22–27 | 21,383 |
| Sharps (a, b) | July 31 | RF04 | ID | 2, 1 | 43.59° | -114.16° | 18.4–19.9 | 50–85 | 26,209 |
| Rabbit Foot (a, b, c) | Aug. 3<br>Aug. 13<br>Aug. 15 | RF06<br>RF10<br>RF11 | ID | 1<br>1<br>5 | 44.86° | -114.27° | 11.2–29.8 | 22–78 | 14,570 |
| Donnell (a, b) | Aug. 6 | RF07 | CA | 1, 2 | 38.36° | -119.88° | 35.7–45.5 | 66–106 | 14,751 |
| Bear Trap (a, b) | Aug. 9 | RF09 | UT | 1, 1 | 39.29° | -109.87° | 11.5–30.6 | 30–74 | 4,955 |
| Dollar Ridge | Aug. 9 | RF09 | UT | 1 | 40.14° | -110.88° | 29.6 | 118 | 27,870 |
| Monument | Aug. 13 | RF10 | MT | 1 | 45.00° | -111.82° | 15.2 | 27 | 2,676 |
| Wigwam | Aug. 13 | RF10 | MT | 1 | 45.14° | -111.89° | 14.4 | 18 | 1,654 |
| Goldstone (a, b) | Aug. 13<br>Aug. 15 | RF10<br>RF11 | MT/ID | 1<br>1 | 45.11° | -113.56° | 13.8–51.9 | 19–121 | 3,787 |
| Beaver Creek (a, b) | Aug. 15 | RF11 | MT | 1, 1 | 45.94° | -113.51° | 27.3–56.2 | 57–127 | 845 |
| Mendocino Complex | Aug. 20 | RF13 | CA | 1 | 39.43° | -122.84° | 57.1 | 120 | 185,804 |
| Red Feather Prescribed Burn (a, b) | Sep. 10 | RF18 | CO | 1, 1 | 40.85° | -105.58° | 3.5–4.8 | 17–17 | 1,759 |
| Silver Creek (a, b) | Sep. 13 | RF19 | CO | 1, 1 | 40.23° | -106.60° | 24.7–27.3 | 23–28 | 8,142 |

387 [a]Letters in parentheses denote smoke plumes sampled more than 30 minutes apart, where each is
388 treated separately in emission factor calculations (Section 2.5). [b]Number of emission transects
389 per fire as denoted by a, b, or c. Emission transect times can be found in Table S6. [c]Total area
390 burned by the fire before being extinguished, sourced from
391 https://www.fireweatheravalanche.org.
392

393 Excess mixing ratios (Δ) for high rate measurements were determined per transect by subtracting
394 the linearly interpolated background between air measured immediately outside both edges of the
395 plume transect as determined by CO and acetonitrile levels. For lower rate measurements by
396 TOGA and AWAS, Δ was calculated using the average background of the samples taken nearest
397 one or both edges of a plume transect.

398

399 ERs were calculated by integrating the background-corrected in-plume measurements and
400 dividing by the plume-integrated CO mixing ratio (averaged over each measurement's sampling
401 time). We note that ERs here are calculated by integrating PTR-ToF-MS and CO real-time
402 plume measurements, rather than using the slope of the least-squares regression of ΔVOC versus

403 ΔCO to better quantify low mixing ratio species and minimize potential biasing ERs by the
404 center or edge of plume measurements.

405

406 EFs were calculated using the carbon mass balance method, assuming all burnt carbon is
407 volatilized and detected following (Yokelson et al., 1999):

408

409 $$EF_{VOC_i}(VOC_i) = F_c \times 1000 \left(\frac{g}{kg}\right) \times \frac{MW_{VOC_i}}{12} \times \frac{\frac{\Delta VOC_i}{\Delta CO}}{\sum_{j=1}^{n}\left(NC_j \times \frac{\Delta VOC_i}{\Delta CO}\right)} \quad (3)$$

410

411 Where $F_c$ is the mass fraction of carbon in the fuel, $MW_{VOC_i}$ is the molecular weight of a given
412 $VOC_i$, 12 is the atomic mass of carbon, $\frac{\Delta VOC_i}{\Delta CO}$ is the ER of $VOC_i$ to CO in ppb ppb$^{-1}$, $NC_{VOC_i}$ is
413 the number of carbon atoms in $VOC_i$, and the sum is over all carbon containing species including
414 161 ions and individual VOCs measured by PTR-ToF-MS, AWAS, TOGA, and $I^-$ CIMS, along
415 with organic carbon (OC), black carbon (BC), CO, $CO_2$, and $CH_4$. We use 45.7 % for the
416 effective fuel carbon fraction for the western U.S. fuels (Santín et al., 2015) as justified by Liu et
417 al. (2017) for computing EFs (Section 6).

418

419 Additionally, to explore the dependence of EFs on the combustion efficiency (Section 7), we
420 calculated the modified combustion efficiency (MCE) for each emission transect using the plume
421 integrated excess CO and $CO_2$ mixing ratios:

422

423 $$MCE = \frac{\Delta CO_2}{\Delta CO_2 + \Delta CO} \quad (4)$$

424

425 **3 Inferred isomeric contribution to PTR-ToF-MS ion masses in fire smoke**

426 The TOGA instrument aboard the C-130 during WE-CAN provides sufficient constraints to
427 quantify the isomeric fractional contributions for four PTR-ToF-MS ion masses using 12 TOGA
428 speciated VOCs measured in 20 emission transects (Figure 1; Table S1). Such isomeric

information fills a gap in PTR-ToF-MS measurements and is rarely available due to limited co-deployed instruments, especially in fire smoke with complex mixtures of VOCs (Section 2.2.2). Koss et al. (2018) found that the isomeric fractional contributions tended to be similar across different fire burns and fuel types during FIREX-MFL. Here we use TOGA measurements to constrain the isomeric contribution to PTR-ToF-MS ion masses and examine consistency with laboratory studies and their natural variability in wildfires.

Figure 1 and Table S1 shows the isomeric contributions for *m/z* 59.049 (acetone and propanal), *m/z* 71.049 (MVK, MACR, and 2-butenal), *m/z* 107.086 (*m*-, *p*-, *o*-xylenes and ethylbenzene), and *m/z* 137.132 (monoterpenes). Two additional ion masses at *m/z* 69.070 and *m/z* 73.065 are also shown. Both the WE-CAN field and FIREX-MFL laboratory measurements indicate MVK is the largest contributor at *m/z* 71.049 (60 ± 9 % (1σ) WE-CAN, 48 % FIREX-MFL) and acetone at *m/z* 59.049 (83 ± 6 % WE-CAN, 100 % FIREX-MFL). The WE-CAN isomeric contributions of *m/z* 107.086 differ the most from FIREX-MFL, but still show some consistency: (*m*, *p*)-xylenes are the major contributor (46 % ± 5 % WE-CAN, 68 % FIREX-MFL) followed by ethylbenzene (36 % ± 6 % WE-CAN, 10 % FIREX-MFL) and *o*-xylene (18 % ± 10 % WE-CAN, 23 % FIREX-MFL) and.

At *m/z* 137.132, four monoterpenes (camphene, α-pinene, β-pinene + myrcene, and tricylene) were measured by TOGA on the C-130. We approximately speciate *m/z* 137.132 using WE-CAN measurements (Section 2.2.1) but note that laboratory burn studies have recently identified more than 30 monoterpene isomers. Among them, the most dominant compounds vary by fuel type, generally including β-pinene, 3-carene, limonene, α-pinene, and camphene (Hatch et al., 2017, 2019). Though we are likely missing key information to fully assign isomeric fractions for monoterpenes measured by PTR-ToF-MS, we do not expect additional speciation to change the total PTR-ToF-MS monoterpene measurement since the calculated sensitivities for additional isomers would be the same due to their identical chemical formula and functionalities (Sekimoto et al., 2017).

458 We do not attempt to fully speciate *m/z* 73.065 because only methyl ethyl ketone (MEK) and
459 butanal were measured by TOGA during WE-CAN, while Koss et al. (2018) suggests a non-
460 negligible amount of 2-methylpropanal (14 %) may be present at this mass in the laboratory burn
461 experiment. Nonetheless, both studies agree that MEK is the dominant species at *m/z* 73.065
462 contributing 80 % ± 2 % during WE-CAN and 85 % during FIREX-MFL.

463

464 PTR-ToF-MS measured isoprene (*m/z* 69.070) is known to have interfering fragments from 2-
465 methyl-3-buten-2-ol (MBO), which is potentially emitted in more abundance biogenically than
466 isoprene in western U.S. coniferous forests (Karl et al., 2012). Figure 1 shows the fractional
467 contribution of isoprene and MBO for the hypothetical case of all MBO fragmenting and being
468 detected at *m/z* 69.069 (i.e., their ratio to the sum of isoprene and MBO). In this scenario *m/z*
469 69.069 would be 93 ± 9 % isoprene, suggesting that in western U.S. wildfire emissions, MBO
470 may not be a significant interfering fragment.

471

472 We find isomeric fractional contributions vary relatively little from fire-to-fire during WE-CAN,
473 with standard deviations across 20 emission transects less than 10 % for half of the isomers
474 shown in Figure 1. Monoterpenes (31–60 %) and MBO (96 %) fractional contributions vary the
475 most between emission transects, likely reflecting changing background levels in the lofted air
476 above the forests. Though these above six ion masses constrained by TOGA are a small sample
477 of all isomeric fractional information needed for PTR-ToF-MS measurements, the little observed
478 fire-to-fire variation hints that the ratios of isomers measured in the laboratory are comparable to
479 similar fuels measured in the field.

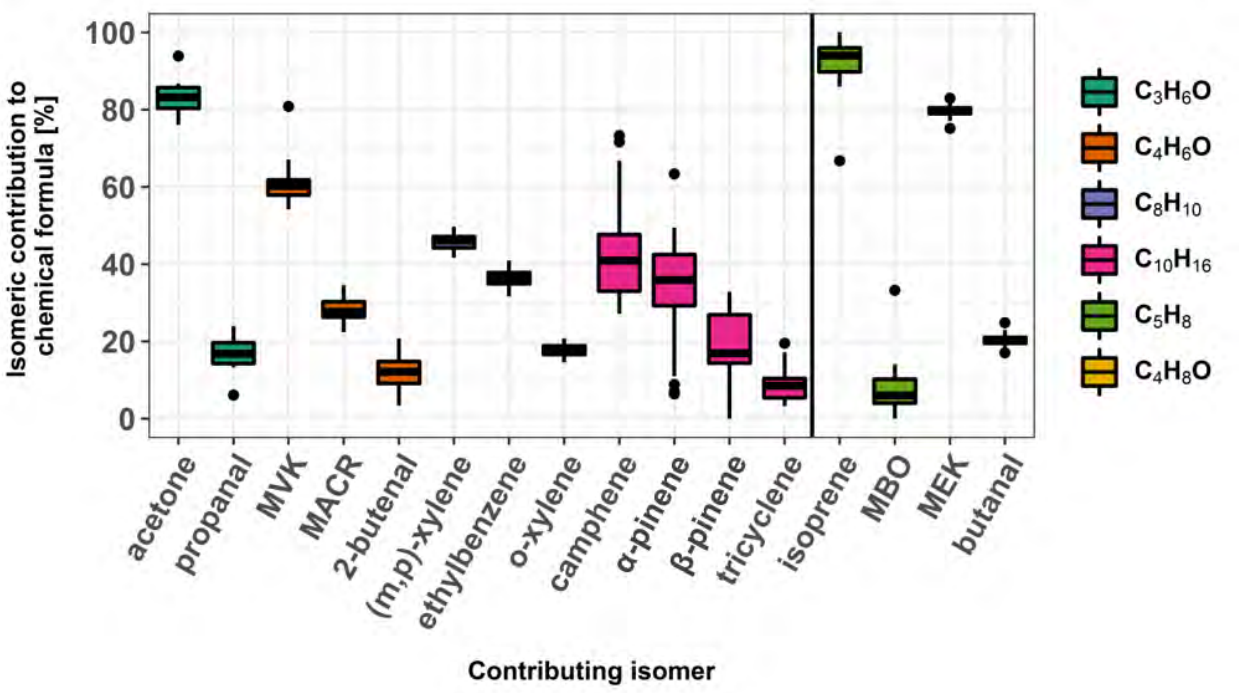


**Figure 1:** Individual isomer contributions to PTR-ToF-MS ions as measured by TOGA from 20 emission transects during WE-CAN. Box and whisker plots (boxes: 25$^{th}$ and 75$^{th}$ percentiles, horizontal line: median, whiskers: 1.5x the inter quartile range, points: > 1.5x inter quartile range) are grouped by color corresponding to a single chemical formula. VOCs to the left of the vertical line were used to speciate four PTR-ToF-MS ion masses in this work. Isoprene and MBO are not isomers but are included due to the potential for MBO to contribute a significant interfering fragment to *m/z* 69.070 in coniferous forests (Karl et al., 2012). MEK and butanal, *m/z* 73.065, are not used for speciation because ~14 % of the signal may be from 2-methylpropanal (Koss et al., 2018), which was not measured aboard the C-130. Note that β-pinene also includes myrcene.

## 4 Instrument intercomparison

Here we compare the co-deployed PTR-ToF-MS, TOGA and AWAS VOC observations during WE-CAN. Though at lower sampling frequencies (Section 2.3), both TOGA and AWAS GC-based measurements observe many VOCs not detected by PTR-ToF-MS while providing additional analytical separation power. We focus on the 24 ‘unique fire’ emission transects and assess the implications for instrument uncertainties for measuring wildfires emissions. Whenever possible, multiple isomers measured by each method are summed together for comparison.

Figure 2 summarizes intercomparison results from the reduced major axis regression between PTR-ToF-MS and the two GC-based instruments. Most of the VOCs directly calibrated by PTR-ToF-MS, with only a single known isomer, and little interference due to fragments (formaldehyde, methanol, acetonitrile, acetaldehyde, benzene, and toluene) agree within combined measurement uncertainties with the GC instruments, typically < 30 %. PTR-ToF-MS calibrated masses with identified contributing isomers or interfering fragments including butenes, acetone/propanal, MVK/MACR/2-butenal, MEK/butanal/2-methylpropanal, ethylbenzene/(*m*,*p*)- and *o*-xylenes (*m/z* 57.070, 59.049, 71.049, 73.064, and 107.085, respectively) also agree within ± 30%.

Notable disagreement is found for five ion masses. PTR-ToF-MS measured isoprene is ~2 times higher than either TOGA or AWAS during smoke sampling. However, when sampling over forested regions with relatively little smoke influence, TOGA, AWAS, and PTR-ToF-MS isoprene agree within the combined uncertainty (not shown). Additionally, the PTR-ToF-MS isoprene shows poor correlation with the two GC instruments ($r^2$= 0.43), which suggests further fragment interference than the 37 % that we removed based on FIREX-MFL results (Koss et al., 2018). As mentioned in Section 3, TOGA typically measured little MBO relative to isoprene in WE-CAN emission transects, thus its fragments are not likely to be the major contributor. Additionally, cyclohexane fragments could play a role (Gueneron et al., 2015; Yuan et al., 2014), though their contribution in wildfire smoke is likely small as TOGA measured isoprene ERs were nearly 12 times higher than cyclohexane measured by AWAS during WE-CAN. Subsequently, the source of any additional fragments in fire smoke is currently unknown.

Total monoterpene abundance measured by PTR-ToF-MS is ~5 times higher than the sum of camphene, α-pinene, β-pinene/myrcene, and tricyclene measured by TOGA. This is likely due to a combination of factors. First, over 30 different monoterpene isomers have been detected in smoke, with the dominant isomers being highly variable between fuels (Hatch et al., 2017, 2019), while only four monoterpene isomers were reported by TOGA during WE-CAN (Figure 1). It is likely a large proportion of monoterpenes were not measured here (Section 3). Second, the PTR-ToF-MS monoterpene sensitivity is weighted by a speciation profile from TOGA

measurements (Section 2.2.2; Eq. (2)). However, the factor of 5 difference here is much larger than can reasonably be explained by differences in calibration factor alone as it would require unrealistic sensitivities. Finally, in addition to other monoterpene isomers, the high PTR-ToF-MS monoterpene measurement may have a contribution from interfering fragments from higher-mass species such as bornyl acetate (Hatch et al., 2017).

PTR-ToF-MS measured furan ~1.5 times higher than TOGA with an $r^2$ of 0.814, potentially suggesting an unknown additional isomer detected by PTR-ToF-MS or a loss in the GC system. Methylfurans were measured by PTR-ToF-MS to be ~15 times greater than the sum of isomers measured by TOGA. Though the PTR-ToF-MS measurement was corrected for being 37 % fragmentary at this mass following Koss et al. (2018), the cause of this discrepancy is currently unknown. Finally, the sum of $C_9$ aromatics measured by AWAS was found to be ~4 times greater than PTR-ToF-MS (not shown in Figure 2 to preserve y-axis scale). As the PTR-ToF-MS was calibrated using 1,3,5- and 1,2,4-trimethylbenzene, this may indicate a significant proportion of other substituted $C_9$ aromatics undergo fragmentation in the drift tube, potentially biasing the PTR-ToF-MS $C_9$ aromatic measurement low.

For PTR-ToF-MS ion masses with only calculated calibration factors, acrylonitrile, propanenitrile, and acrolein measured by TOGA were found to agree within the combined measurement uncertainty of < 60 %. AWAS measured propene was observed to be 2.5 times higher than measured by PTR-ToF-MS, potentially due to overcorrecting the amount of that mass attributed to fragments (not shown in Figure 2 to preserve y-axis scale). TOGA-measured styrene was found to be ~4 times lower than PTR-ToF-MS, and the reason for this discrepancy is currently unknown. AWAS propene and TOGA styrene are reported in this work rather than PTR-ToF-MS (Section 2.4).

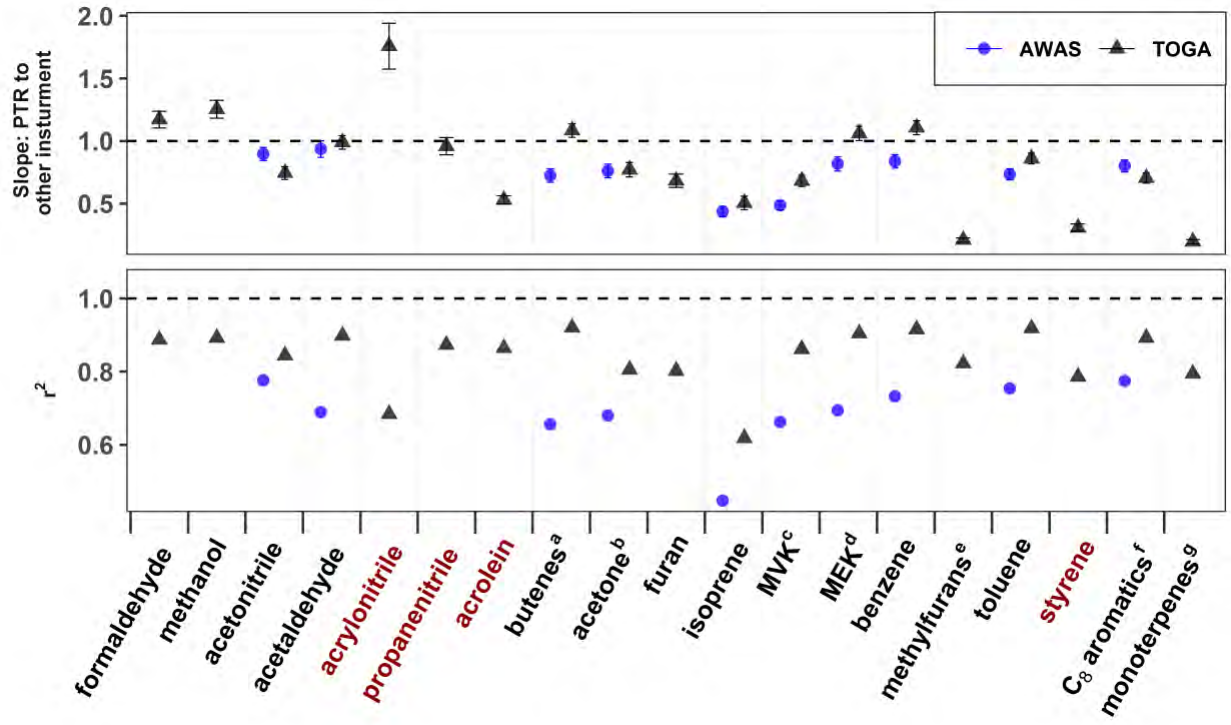


**Figure 2.** Slope and correlation coefficients ($r^2$) of the reduced major axis regression of PTR-ToF-MS versus TOGA (blue circles) and AWAS (black triangles) mixing ratios for all available emission transect measurements used in this work (~34 TOGA samples and ~40 AWAS samples). Error bars show the standard error of the slope, often too small to be discernible behind the points. VOCs in red have calculated PTR-ToF-MS calibration factors (Sekimoto et al., 2017), while VOCs in black have at least one directly calibrated isomer. Names for the most abundant VOC for each chemical formula are shown while superscripts denote VOCs where multiple isomers measured by TOGA or AWAS are summed together for comparison to the PTR-ToF-MS measurement. [a]TOGA: isobutene, 1-butene; AWAS: 1-butene, cis-2-butene, and trans-2-butene. [b]TOGA: acetone and propanal; AWAS: acetone. [c]TOGA: MVK, MACR, 2-butenal; AWAS: MVK and MACR. [d]TOGA: MEK and butanal; AWAS: MEK. [e]TOGA: 2-methylfuran and 3-methylfuran. [f]TOGA: (*m*,*p*)-xylenes, ethylbenzene, and *o*-xylene; AWAS: (*m*,*p*)-xylenes, ethylbenzene, and *o*-xylene. [g]TOGA: camphene, α-pinene, β-pinene + myrcene, and tricylene.

Due to different sampling frequencies, TOGA and AWAS mixing ratios cannot be directly compared as in Figure 2. Instead, we compare ERs for 15 'unique fires' where both TOGA and AWAS capture the same plume transect (Figure S3). All TOGA and AWAS co-measured ERs except $C_8$ alkanes agree within < 50 %, with most < 20 %. AWAS measured $C_8$ alkanes ERs ~2 times higher than TOGA, likely due to the inclusion of AWAS octane, 2,2,4-trimethylpentane, and 2-methylheptane ERs relative to just octane measured by TOGA. Though slopes for the reduced major axis regression between TOGA and AWAS ERs agree well, correlation

coefficients and standard errors are generally worse than in Figure 2 due to added uncertainty from the CO measurement, background corrections, and sampling of different locations within a plume.

During WE-CAN, 48 % of measured mass (sum of VOC emission factors) was directly calibrated in the PTR-ToF-MS, emphasizing that the strength of the technique is largely dependent on the ability to get accurate sensitivities for non-directly calibrated VOCs. PTR-ToF-MS is further challenged by a lack of speciation information for wildfire smoke, which likely contributes to discrepancies when comparing to TOGA or AWAS measurements (Figure 2). However, the high temporal resolution (< 1 s) of PTR-ToF-MS allows for narrow smoke plumes with rapid changes in VOC concentrations to be captured (Müller et al., 2016), while TOGA is constrained by the time needed for gas chromatography separation (~100 s). Though AWAS theoretically has little temporal limitations between filling consecutive canisters, the discrete number of canisters available per flight makes it difficult to capture every plume transect while still sufficiently characterizing background air. As most plumes were only 1–4 minutes wide at the emission transect and most flights had tens or more transects through smoke, of the 31 emission transects identified in this work only 20 were sampled by TOGA and 20 by AWAS. Together, the large number of VOCs measured by PTR-ToF-MS, coupled with the speciation power, low detection limits, and characterization of alkanes, alkenes, nitrogen containing VOCs and halides of AWAS and TOGA greatly improves our ability to characterize wildfire emission during WE-CAN. If each instrument were deployed to sample fire emissions alone, a PTR-ToF-MS would capture 87 % of the measured mass during WE-CAN (Section 7.2), while AWAS and TOGA capture 34 % and 38 % respectively. These proportions are somewhat consistent with the proportions reported from laboratory burns (Hatch et al., 2017). Of the fraction captured by AWAS, 65 % are alkenes, aldehydes, and alkanes. Similarly, 65 % of the TOGA fraction consists of aldehydes, alcohols, and aromatics.

## 5 Emission factors for speciated and total VOCs

Table 2 shows WE-CAN campaign-averaged emission ratios and emission factors for 161 ion masses, individual VOCs, OC, BC, $CH_4$, CO, and $CO_2$. Additional speciation is provided for 30

isomers known to contribute to PTR-ToF-MS ions masses (Section 2.4). Fire-to-fire variability is reflected by the standard deviation of the study average (1σ). A more detailed breakdown of EFs and ERs by fire can be found in the supplement (Tables S2 and S3). Emission information for $NH_3$, $NO_x$, and other reactive nitrogen species measured during WE-CAN can be found in Lindaas et al. (in review) and Peng et al. (2020). Emission ratios for organic aerosol are available in Garofalo et al. (2019).

For the western U.S. wildfires sampled during WE-CAN, the total measured mass of VOCs emitted per fire (expressed as the total emission factor of all measured VOCs, or $tVOC_{EF}$) ranges from 9.8 g $kg^{-1}$ to 35.9 g $kg^{-1}$, with a mean emission factor of 26.1 ± 6.9 g $kg^{-1}$ (1σ). Our average $tVOC_{EF}$ is consistent with many previous studies including (1) an early estimate of total non-methane organic gases (NMOG) for temperate forest fires (23.7 g $kg^{-1}$) from Akagi et al. (2011), (2) total NMOG for pine-forest understory prescribed fires (27.6 g $kg^{-1}$) from Yokelson et al. (2013), (3) total NMOG from FLAME-4 laboratory coniferous canopy fires (23.9 g $kg^{-1}$) in Stockwell et al. (2015; Table 1), and (4) the total PTR-ToF-MS measured NMOG for carefully simulated wildfires in FIREX-MFL (25.0 g $kg^{-1}$; Koss et al., 2018).

On a molar basis, the total measured VOC emitted by western U.S. wildfires relative to CO (sum of ERs) ranges from 90.0 ppbv $ppmv^{-1}$ to 206.1 ppbv $ppmv^{-1}$, with an average of 148.3 ± 29.6 ppbv $ppmv^{-1}$. This sum of ERs is also similar to the laboratory-determined sum of 144.5 ppbv $ppmv^{-1}$ for western U.S. fuels (Koss et al., 2018). We later conduct a detailed comparison with previous field and laboratory studies exploring the ability of flaming versus smoldering combustion processes to explain variability in total measured VOC emissions (Section 7).

On average, the top 10 most abundantly emitted species groups account for ~53 % of the $tVOC_{EF}$ in western U.S. wildfire smoke, or ~68 % on a molar basis (Figure 3). The remaining 47 % of VOC mass is represented by at least 151 species groups, each individually contributing less than 2 % to the overall $tVOC_{EF}$. In contrast, 15 species groups were needed to reach 50 % of the total measured VOC emissions in FIREX-MFL (Koss et al., 2018), likely due to the inclusion of

637 ethane in this work, as well as the higher acetaldehyde, ethene, formic acid, and acetone EFs
638 observed during WE-CAN relative to FIREX-MFL. Many of the most abundantly emitted VOC
639 groups have also been reported as top emissions in other field and laboratory studies, though
640 some may be in varying orders of abundance (Akagi et al., 2011; Hatch et al., 2017; Koss et al.,
641 2018; Liu et al., 2017; Müller et al., 2016; Selimovic et al., 2018). For example, Akagi et al.
642 (2011) reported the sum of acetic acid and glycolaldehyde (2.22 g $kg^{-1}$) essentially equal with
643 formaldehyde as the most abundant VOC from temperate forest fires, similar to FIREX-MFL
644 (2.6 g $kg^{-1}$) (Selimovic et al., 2018) and WE-CAN (2.4 ± 0.59 g $kg^{-1}$).

645

646 Of important exception, total monoterpenes have been measured in laboratory burns as among
647 the most abundantly emitted VOCs (Akagi et al., 2011; Hatch et al., 2017; Koss et al., 2018),
648 however, they do not rank in the top 30 in WE-CAN EFs (0.2 g $kg^{-1}$), nor the top 10 reported in
649 another aircraft study of western fires (Liu et al., 2017) or southeastern U.S. prescribed fires
650 (Müller et al., 2016). Akagi et al. (2013) found that some major monoterpene EFs determined
651 from airborne measurements directly over prescribed fires were significantly lower than those
652 from ground based samples of the same fires. This may be in part because these monoterpenes
653 tend to be produced from fuels (e.g., dead/down logs) that release emissions with less tendency
654 to be lofted into the main convective column of the plume and sampled by aircraft. Additionally,
655 airborne measurements by larger aircraft such as the NSF/NCAR C-130, may only be possible
656 several minutes downwind of the flame front, thus highly reactive species such as monoterpenes
657 could have undergone some extent of chemical removal before being sampled.

658

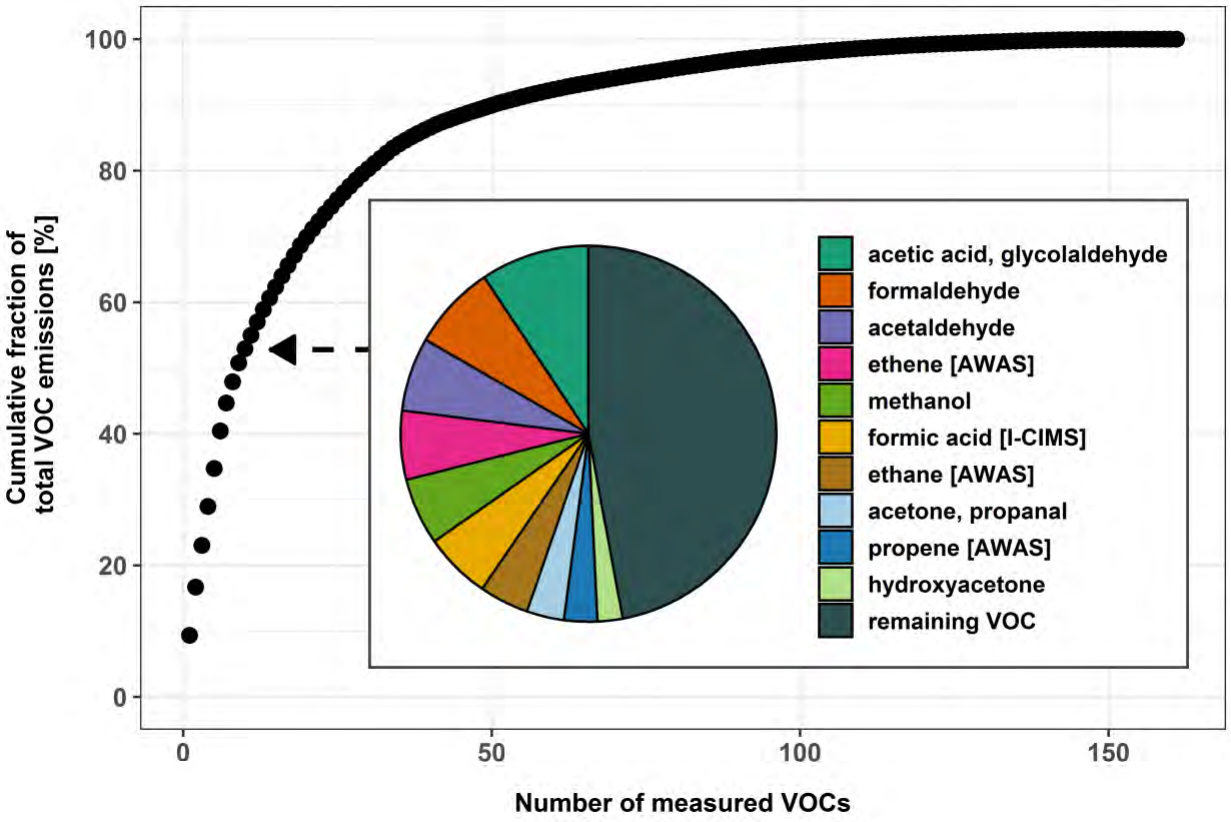


**Figure 3.** The cumulative mass fraction of the total measured VOC emissions as a function of measured VOCs during WE-CAN. 76 VOC groups account for 95% of the total measured VOC mass, and 117 VOC groups account for 99 % of the total measured VOC mass. The inset pie chart shows the ten most abundantly emitted VOC groups which account for ~53 % of the total mass emitted, while the remaining mass consists of 151 species. Reported species not measured by PTR-ToF-MS are identified by corresponding instrument in the legend (i.e., Ethene [AWAS]). Note that hydroxyacetone also includes methyl acetate and ethyl formate isomers (Koss et al., 2018).

Oxygen containing VOCs were found to contribute 67 % of the $tVOC_{EF}$ (or 61% on a molar basis). It is approximately 5–10 % higher than previous comprehensive laboratory studies of western U.S. fuels (51–57 % of the total on a molar basis; Gilman et al., 2015; Hatch et al., 2017; Koss et al., 2018), potentially reflecting oxidation of VOC emissions before being sampled by the C-130.

## 6 Comparison to previous studies

In this section, we compare the WE-CAN campaign averaged EFs to past studies. Four relevant studies were selected: two PTR-ToF-MS laboratory studies of simulated burns representative of western U.S. fuels (Koss et al., 2018; Stockwell et al., 2015), airborne measurements of wildfire EF (Liu et al., 2017), and one compilation of temperate forest fire EFs based mainly on pine understory prescribed fires (Akagi et al., 2011). Here we examine differences between field and laboratory measured EFs across individual species in the context of natural fire-to-fire variability and later explore potential explanations for the observed variability in Section 7.

Figure 4 compares WE-CAN EFs for the top 20 most abundantly emitted VOC groups (~70 % the measured $tVOC_{EF}$) and the sum of remaining VOCs for the 24 'unique fires' sampled more than 30 minutes apart (Table 1). The WE-CAN VOC EFs in a logarithmic scale reveals the large species-to-species and fire-to-fire variability of observed EFs, which except for formic acid and acrolein, overlap the literature values for similar fuels. Formic acid EFs measured by both $I^-$ CIMS and PTR-ToF-MS (not shown) were higher than the laboratory and synthesis studies, which may be related to the rapid formation in fresh fire plumes (Akagi et al., 2012). WE-CAN acrolein EFs are consistently lower than in the laboratory, which may reflect chemical loss prior to airborne sampling. Though WE-CAN EFs largely overlap literature values, there are many individual data points where one or more studies are > 1.5 times the interquartile range of the WE-CAN EF, emphasizing the need for multiple biomass burning emission measurements to improve EF statistics.

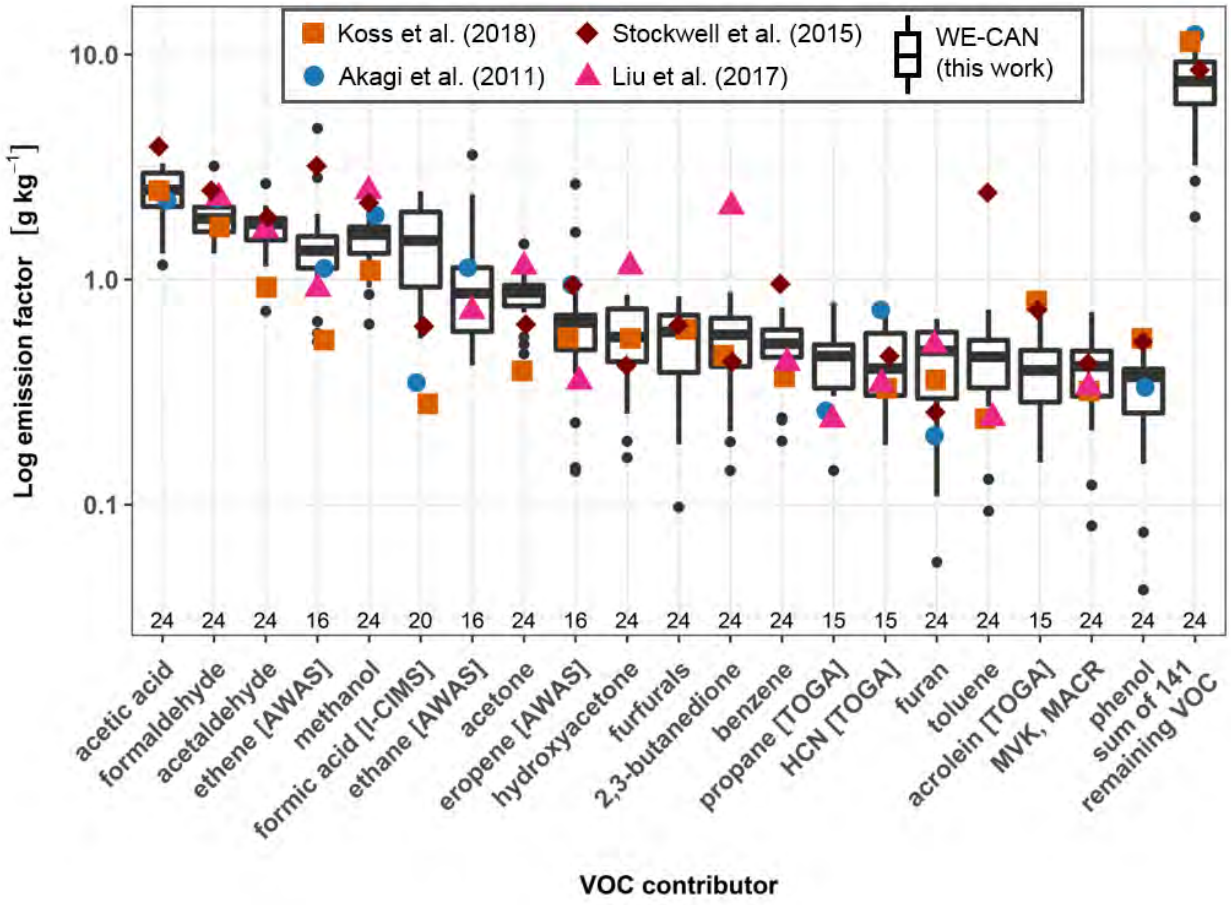


**Figure 4.** Box plot of emission factors for the 20 most abundantly emitted and remaining VOCs by mass during WE-CAN. The number of 'unique fire' EFs (Table 1) used for each box is shown at the bottom of the plot. Also shown are relevant literature values for western U.S. fuel types. Specifically, the Akagi et al. (2011) value shown with the "sum of 147 remaining VOC" is the total non-methane organic carbon (NMOC) for temperate forests, excluding the EFs shown for individual VOCs. The Stockwell et al. (2015) values are the average EFs for relevant western U.S. fuels measured by PTR-ToF-MS and Fourier-transform infrared spectroscopy (FTIR; 4 black spruce, 2 juniper, and 7 ponderosa pine fueled laboratory burning experiments), weighted by the number of reported burns. The Koss et al. (2018) values are FIREX-MFL western U.S. fuel type study averages, while Liu et al. (2017) reports average EFs of three western U.S. wildfires sampled during the Biomass Burning Observation Project (BBOP) and the Studies of Emissions and Atmospheric Composition, Clouds, and Climate Coupling by Regional surveys (SEAC$^4$RS) aircraft campaigns. TOGA, AWAS, and $I^-$ CIMS measurements are noted in brackets. PTR-ToF-MS measured species names reflect the most abundant isomer at that mass (Koss et al., 2018), and is consistent with the compared literature. Note that $C_2H_4O_2$: acetic acid includes glycolaldehyde, $C_3H_6O$: acetone includes propanal, $C_3H_6O_2$: Hydroxyacetone includes methyl acetate and ethyl formate, $C_5H_4O_2$: furfurals include 2-furfural and 3-furfural, $C_4H_6O_2$: 2,3-butanedione includes methyl acrylate, and $C_4H_6O$: MVK, MACR includes 2-butenal.

716 Detailed speciation information is available in Table 1.
717
718 Figure 5 further compares WE-CAN EFs for 116 species measured by PTR-ToF-MS to the
719 FIREX-MFL laboratory experiment average (Koss et al., 2018). Reduced major axis regression
720 between the two campaign averages shows good agreement with a slope of 0.93 and $r^2$ of 0.82.
721 The large fire-to-fire variability of WE-CAN measured EFs is again apparent, with many WE-
722 CAN individual fire EFs potentially lower than the FIREX-MFL at the higher EFs, while the
723 opposite trend exists at lower values.

724

725 To quantify the fire-to-fire EF variability, we focus on PTR-ToF-MS (and $I^-$ CIMS)
726 measurements to prevent statistical bias from the smaller TOGA and AWAS sample sizes. Of
727 these, the median fire-to-fire EF coefficient of variation (COV, standard deviation divided by the
728 mean) is 43 % (45 % mean; Table 2). Nitromethane, formaldehyde, isocyanic acid, and acetic
729 acid have the least variable EFs with COVs of 11–25 % for the campaign and ranges varying by
730 less than a factor of 3. Conversely, the most variable species are some of the most reactive
731 (monoterpenes, creosol, vanillin, and sesquiterpenes; COV 73–108 %), suggesting a potential
732 role of rapid early plume chemistry in the observed variability. The "sum of remaining VOCs"
733 further characterizes the variability, ranging by nearly a factor of 4 across all fires with 29 %
734 COV (a factor of 2 and 23 % COV on a molar basis).

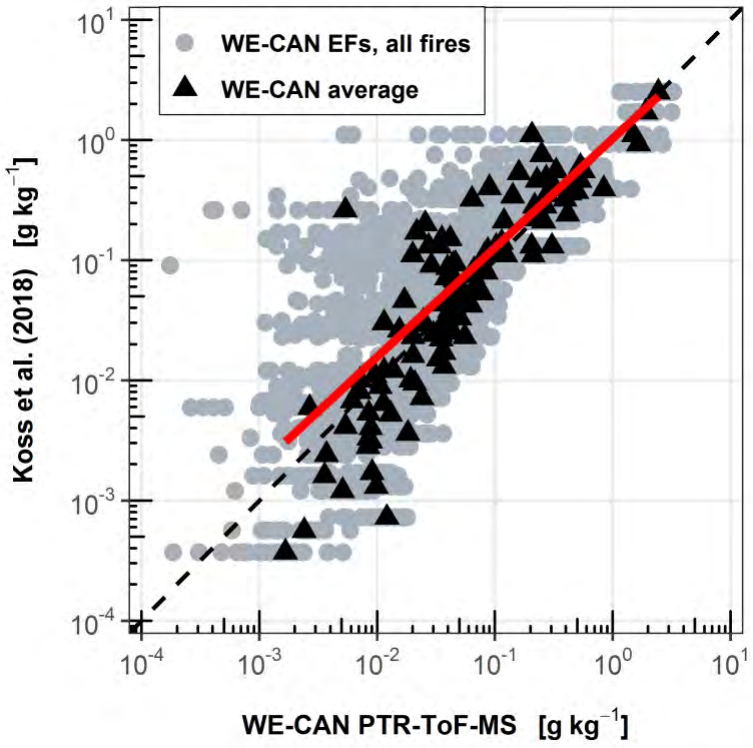


735

736 **Figure 5:** WE-CAN campaign averaged (black triangles) and individual fire (grey points) EFs
737 compared to study average EFs reported by Koss et al. (2018) for 116 species measured by PTR-
738 ToF-MS. The dashed line represents one-to-one agreement, while the reduced major axis
739 regression of the two study averages is shown by the solid red line. Average EFs measured in the
740 two studies show good agreement, while EFs for all fires show the large fire-to-fire variability of
741 WE-CAN emissions.

742

743 **7 Dependence of emission factors on the modified combustion efficiency**

744 Though direct comparisons of campaign averaged EFs as in Figures 4 and 5 are common in the
745 literature for showing agreement between studies, such comparisons largely ignore the
746 dependence of EFs on combustion processes. In this section, we explore the relationship between
747 MCE and EFs for all measured VOCs in an attempt to explain some of the observed variability
748 and relate WE-CAN observations to the growing EF literature with the simple combustion proxy
749 that is readily measured in the field.

750 7.1 Individual VOC emission

751 Figure 6 shows that 98 out of 151 reported VOC EFs, measured in at least 10 of the 24 fires,
752 correlate to MCE with p-values < 0.05, indicating that 76 % of the average $tVOC_{EF}$ has

753 statistically significant dependence on burning conditions. Of these, correlation coefficients
754 range from 0.23 for quinone to 0.91 for benzene and all slopes are negative. The wide range of
755 correlation coefficients suggests MCE is not the only contributor to the emission variability, with
756 fuel types, plume aging, and pyrolysis temperature likely playing a role (Roberts et al., 2020;
757 Sekimoto et al., 2018). Still, the correlations obtained by WE-CAN can provide observational
758 constraints on uncertainties for predicting VOC emissions with MCE, particularly for those
759 species that are rarely measured in the field. Overall, we find that MCE can explain at least 50 %
760 of the variance for 57 individual VOC EFs, representing 54 % of the $tVOC_{EF}$. Equations and
761 coefficients for these 98 correlations are listed in the supplement (Table S1).
762

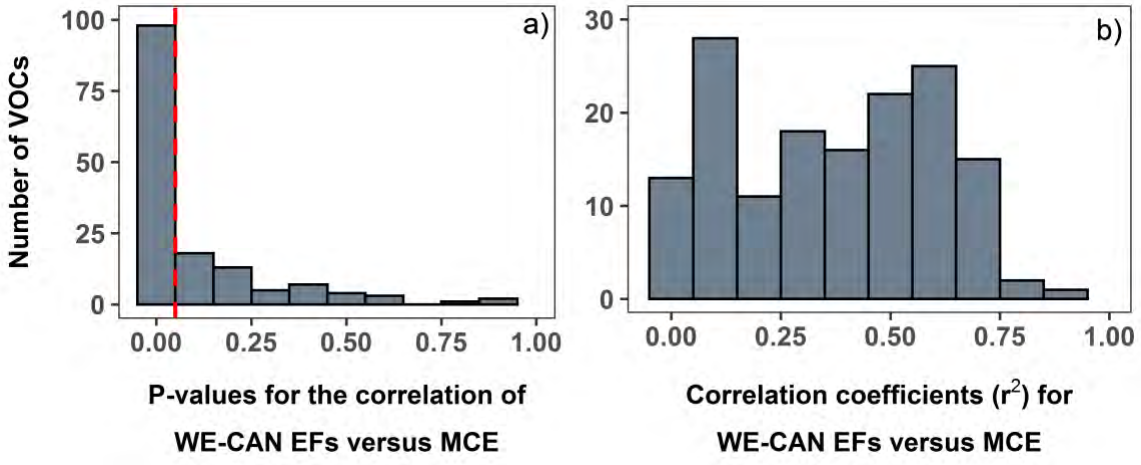

763

764 **Figure 6:** a) Histogram of p-values from the least squares regression of EF versus MCE for 151
765 VOCs. Among them, 98 VOC EFs have a statistically significant correlation with MCE, p-values
766 < 0.05, represented by the red dashed line. b) The same as Panel a) except for correlation
767 coefficients ($r^2$) of the least squares regression of EF versus MCE.
768

769 We compare WE-CAN EFs to previous studies in terms of their dependence on MCE for $CH_4$
770 and five VOCs selected for their representativeness as discussed below. Figure 7 shows that
771 when MCE is considered, WE-CAN EFs show good agreement with both laboratory and field
772 measurements, with slightly better agreement with field data. Benzene, methanol, and $CH_4$
773 represent long-lived species with minimal degradation in the plume aging times characteristic of
774 the WE-CAN emission transects. Interestingly, the spread in the laboratory benzene EFs are
775 larger than the field data. Furan and furfurals represent shorter-lived species, while acetaldehyde
776 is a photochemical product of many VOCs. Finally, $CH_4$ also highlight agreement between EFs

measured by one of the non VOC instruments used in this work. Although the comparison of these six species is not inherently representative of the other 156 VOC reported in this work, they do suggest that WE-CAN measured EFs agree with previous studies when compared in the context of MCE. Additionally, Figure 7 highlights that despite complex fuels and combustion chemistry, the simple MCE index explains a significant amount of the study-to-study variability, though remaining variance is expected due to fuel chemistry, moisture, geometry, etc (Yokelson et al., 1996).

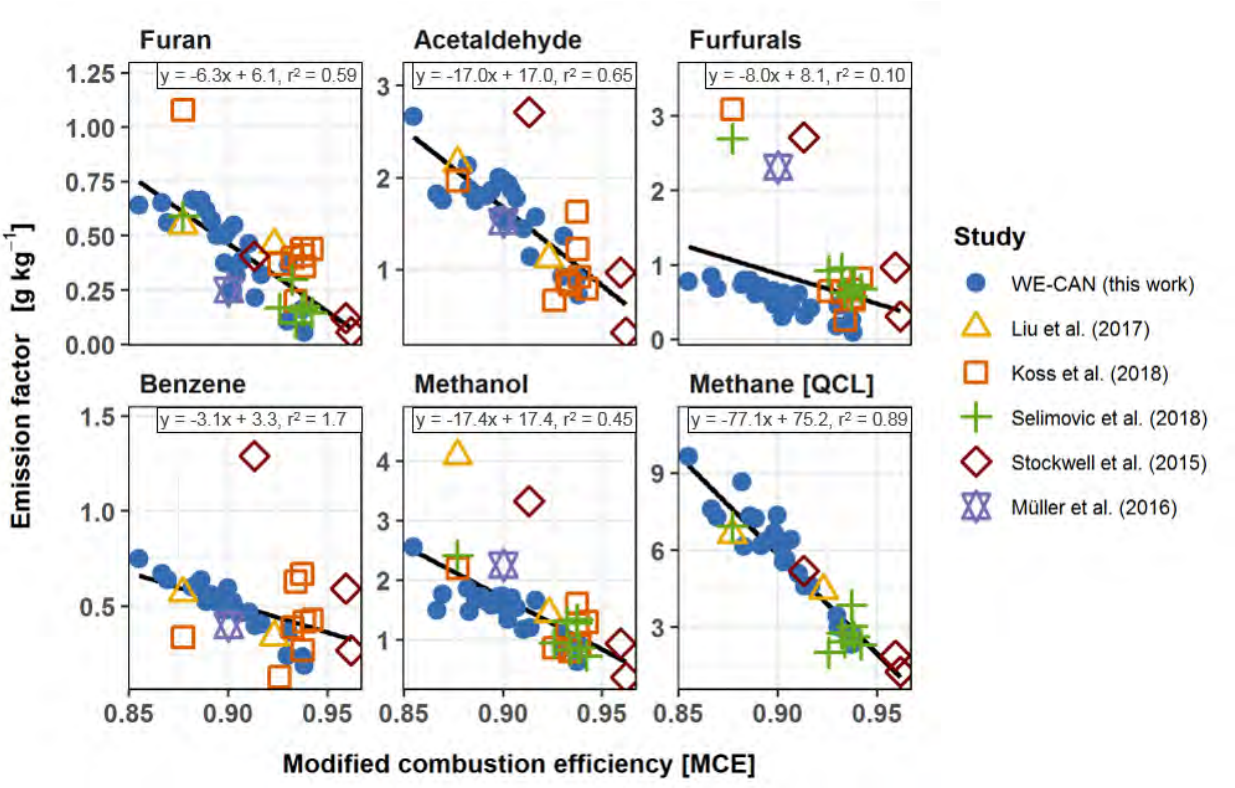


**Figure 7:** Correlations of EFs versus MCE for methane and a subset of VOCs (furan, acetaldehyde, furfurals, benzene, and methanol) commonly reported in the literature. Also shown are additional EFs for two field campaigns (Liu et al., 2017; Müller et al., 2016) and coniferous fuels measured during three laboratory burns (Koss et al., 2018; Selimovic et al., 2018; Stockwell et al., 2015). Black lines represent the least squares regression for all studies. Regression statistics of all 151 VOC EFs with MCE are available in Table S5.

### 7.2 Total measured VOC emissions

WE-CAN total measured VOC emissions strongly correlate with MCE ($r^2 = 0.67$; Figure 8), indicative of less VOC being produced relative to $CO_2$ as fuels burn more efficiently and that

795 nearly 70% of $tVOC_{EF}$ can be explained by MCE alone. Total measured VOC emissions for
796 western U.S. fuels measured during laboratory burns also show a strong negative correlation
797 with MCE ($r^2$= 0.72), however with a much steeper slope and approximately 2 times greater
798 $tVOC_{EF}$ than WE-CAN at similar MCEs. Overall, such strong correlations observed both in field
799 and laboratory studies suggest that total measured VOC emissions could be predicted when the
800 MCE information is available, and individual VOC emission could be subsequently derived
801 using emission profiles (Section 8), similar to the wildland fire portion of the EPA's National
802 Emission Inventory (Baker et al., 2016; U.S. Environmental Protection Agency, 2020)

803

804 There are a few potential reasons for the differences between the WE-CAN and laboratory
805 measured $tVOC_{EF}$. First, rapid chemistry taking place in the wildfire plumes prior to their
806 sampling by the C-130 could result in lower EFs compared to laboratory studies particularly for
807 shorter-lived species, which also tend to have high molecular weights. Similarly, condensation of
808 lower volatility species between emission and sampling may also account for some of the mass
809 difference as ground-based studies of wildfire $\Delta PM_{2.5}/\Delta CO$ ratios show that considerable
810 evaporation of biomass burning organic aerosol occurs at the warmer temperatures typical of the
811 surface or indoor environments (Selimovic et al., 2019). Second, the close proximity of sample
812 inlets to the fires in a laboratory burn likely means that they capture some emissions from
813 smoldering combustion which may not be as efficiently lofted in the wildfire plume and thus
814 underreported in the field. Third, in this work we assume 45.7 % emitted carbon in our carbon
815 mass balance for deriving EFs following other field studies in the western U.S., which contrasts
816 with the ~50 % used during the laboratory studies (Koss et al., 2018; Stockwell et al., 2015),
817 meaning WE-CAN EFs are generally expected to be ~10 % lower (Eq. 3). Additionally, WE-
818 CAN emission factors were calculated using the sum of carbon from 161 ions and individual
819 VOCs, along with OA, BC, CO, $CO_2$, and $CH_4$ for the total carbon term of the mass balance
820 equation (Eq. 3), which is expected to result in slightly lower individual EFs than if a smaller
821 sampling of VOCs, CO, $CO_2$, and $CH_4$ are only used. Fourth, the data available to calculate MCE
822 differs substantially between laboratory and field experiments. In the lab, the full progression of
823 a fire from ignition to completion is measured, and MCE is therefore calculated using the fire
824 integrated CO and $CO_2$ measurements, providing the fires overall MCE for the entirety of the
825 burn. In the field, MCE is calculated from a single transect through a smoke plume which is

826 assumed to contain all the stages of burning. Finally, partly because of fuels drying out before
827 being burned, laboratory studies tend to have higher MCE than wildfires (Christian et al., 2003;
828 Holder et al., 2017; Selimovic et al., 2018; Yokelson et al., 2013). It is likely a combination of
829 the above factors contributes to the difference in $tVOC_{EF}$ versus MCE between field data and
830 laboratory burns.

831

832

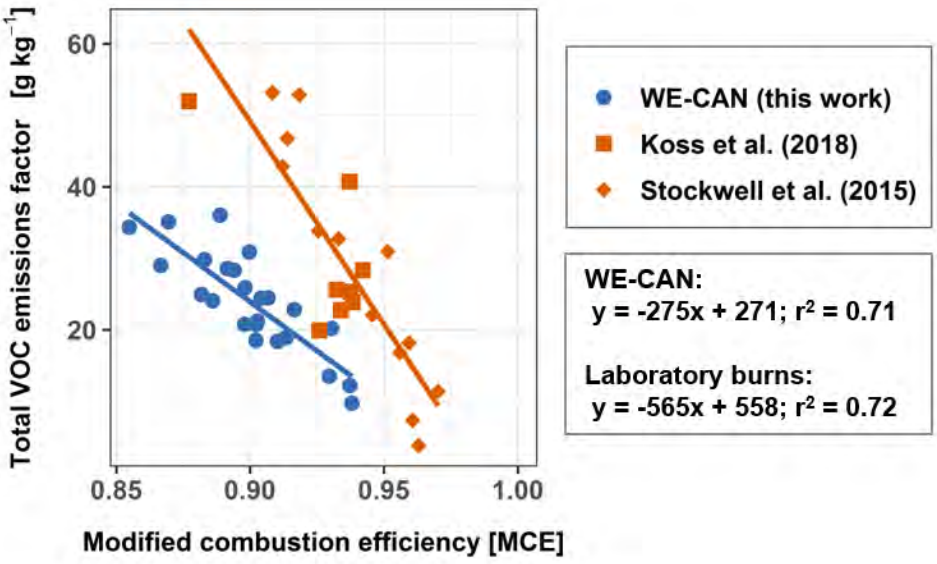


833

834 **Figure 8:** Relationship between total measured VOC emissions and MCE observed in WE-CAN.
835 Also shown are data from laboratory burns for similar fuels during FLAME-4 and FIREX-MFL.
836 The solid lines are corresponding least squares regression fits. WE-CAN total measured VOC
837 emissions include the 161 VOC EFs reported in this work. Koss et al. (2018) total VOC include
838 ~154 PTR-ToF-MS measured ions, excluding ammonia and nitrous acid, from individual burns
839 of ponderosa pine, lodgepole pine, Douglas fir, subalpine fir, Engelmann spruce, loblolly pine,
840 Jeffrey pine, and juniper fuel types. Stockwell et al. (2015) total measured VOC emissions
841 include ~55 PTR-ToF-MS measured ions reported as positively identified and 10 VOCs
842 measured by Fourier-transform infrared spectroscopy (FTIR) during 4 black spruce, 2 juniper,
843 and 7 ponderosa pine fueled laboratory burning experiments.

844

845 Rapid early plume chemistry can cause aircraft-measured EFs of reactive primary VOCs to be
846 lower than at the source, while simultaneously increasing EFs for secondary species. Field and
847 laboratory measured MCEs also differ, making the decision of which EFs to use in models
848 counterintuitive. Generally, laboratory burns may better capture the emissions of reactive VOCs

and emissions representative of smoldering combustion. However, WE-CAN sampled western U.S. wildfires mid-afternoon during the summer, when presumably the fires are burning at their highest emissions production level. Within this dataset, only 4 out of the 24 'unique fires' were characterized by MCE > 0.92, which is at the lower end of MCEs typically reported for laboratory burns of similar fuels. Airborne measurements would be expected to favor flaming combustion, if they have a bias, so a lower MCE in the air suggests a possible bias towards unrealistically high MCE in the lab. For this reason, many laboratory studies provide EFs adjusted to reflect the field average MCE (Selimovic et al., 2018). Interestingly, aging effects may reduce the airborne EFs to levels that are perhaps more appropriate for the spatial resolution of many regional to global models, but it is not simple to rule out the potential loss of smoldering emissions in field sampled fires (Bertschi et al., 2003). Overall, using data from real wildfires makes sense, but lab studies can help characterize species rarely or not measured in the field, especially if they are adjusted to match field MCE or other steps are taken to increase representativeness (Selimovic et al., 2018; Yokelson et al., 2013).

## 8 VOC emission profiles for emissions speciation

Rather than using correlations with MCE to predict individual VOC EF, another approach to get speciated emissions is by applying a flaming or smoldering profile to the total VOC emissions (U.S. Environmental Protection Agency, 2020). We calculate VOC emission profiles by dividing individual VOC EFs by the $tVOC_{EF}$ to get the mass fraction of each species to the total emissions. The dependence of the mass fraction on MCE is then investigated for the same 151 species, measured in 10 or more fires, as in Section 7.1. In contrast to EF versus MCE correlations, we find that only 44 of the 151 reported species have a statistically significant dependence on MCE (p-values < 0.05) with correlation coefficients ranging from 0.17 to 0.62. These 44 VOCs account for 31 % of the average $tVOC_{EF}$. Additionally, 11 of these correlations have positive slopes, with three of the steepest being for formic acid, formaldehyde, and isocyanic acid, indicating that these VOCs account for more of the $tVOC_{EF}$ as combustion efficiency increases.

To further examine the role of MCE on emission profiles, we bin the five highest and five lowest MCE fires sampled during WE-CAN into a "high" and "low" MCE profile. A Wilcox rank-sum

879 test comparing the two profiles shows that only 26 VOCs, ~18 % of the $tVOC_{EF}$, are statistically
880 different between the profiles (p-values < 0.05); among them, only 3 VOCs (methylpyridines,
881 isocyanic acid, and toluene) have p-values < 0.01. This suggests that for the majority of VOCs (>
882 80 % by mass) emitted in western U.S. wildfires, mass fractions of individual VOCs
883 significantly overlap for the MCE range sampled during WE-CAN. As such, separated high and
884 low MCE profiles cannot be clearly defined here and a single campaign averaged VOC emission
885 profile best describes the data for all but a few species (Table 2).

886

887 Recently it has been shown that laboratory biomass burning VOC emissions can be described by
888 two positive matrix factorization (PMF) factors related to high and low temperature pyrolysis,
889 where pyrolysis is one component of smoldering combustion (Sekimoto et al., 2018; Yokelson et
890 al., 1996). One possible explanation for the lack of distinct high and low MCE emission profiles
891 in this work is that emissions from all types of burning (including flaming, gasification, and high
892 and low temperature pyrolysis) are lofted into the large wildfire plumes sampled during WE-
893 CAN (Andreae & Merlet, 2001), which likely results in the high and low MCE emissions
894 intermixing such that the measured VOC profile regresses towards a mean. This result may be
895 different if examined over a broader range of MCEs, such that a direct comparison between
896 smoldering and flaming emissions can be separated.

897 **9 Conclusion**

898 We present emission factors and emission ratios for 161 ions and individual VOCs for western
899 U.S. wildfires measured by complementary instruments onboard the NSF/NCAR C-130 aircraft
900 during the WE-CAN field campaign. In situ emission measurements were made during 31
901 emission transects of 24 'unique' wildfires, significantly expanding the number of observations
902 of many VOCs rarely reported in the field and allowing us to assess the large natural variability
903 of wildfire emissions. Across all fires, measured MCEs ranged from 0.85 to 0.94 when they are
904 typically burning most actively in the mid-to-late afternoon.

905

906 Using co-deployed TOGA measurements for 13 speciated VOCs, we found that the fractional
907 contribution of isomers to four PTR-ToF-MS measured ions (*m/z* 59.049, 71.049, 107.086, and

137.132) had relatively little fire-to-fire variability and were comparable to results in previous laboratory burn experiments for similar fuels. Among 45 co-measured VOCs, 36 showed agreement within combined instrument uncertainties (< 60 %). Disagreement was found between five PTR-ToF-MS ion masses and the two GC-based measurements (*m/z* 69.069 isoprene, *m/z* 69.033 furan, *m/z* 83.049 methylfurans, *m/z* 121.061 $C_9$ aromatics, and *m/z* 137.132 monoterpenes), likely reflecting additional unknown isomers or fragment products detected by PTR-ToF-MS in fire smoke. TOGA and AWAS measurements agree between all co-measured species with the exception of $C_8$ alkanes, where AWAS detected more isomers than TOGA.

The total observed VOC emissions averaged 26.1 ± 6.9 g $kg^{-1}$ (148.3 ± 29.6 ppbv $ppmv^{-1}$) for western U.S. wildfires, consistent with previous studies. The top 10 most abundant VOC groups accounted for 53 % of the total measured VOC mass; while the remaining 47 % was represented by at least 151 species groups, each contributing less than 2 % to the total. Oxygenated VOCs contributed to 67 % of the measured total VOC emissions by mass, or 61 % on a molar basis.

When MCE is considered, we found overall good agreement between individual VOC EFs and previous laboratory and field studies. However, for a given MCE, total measured VOC emissions are nearly 2 times lower than measured in two recent laboratory experiments utilizing similar instrumentation and fuels. The source of this difference may reflect aging effects, fuel differences, or different integration of combustion processes, with laboratory experiments likely biased towards flaming processes. WE-CAN observations reveal 98 species, accounting for 76 % of the average total measured VOC mass, have statistically significant and negative dependences on MCE. VOC mass fractions show much less MCE dependence with significant overlap within the observed MCE range, suggest that a single speciation profile can describe VOC emission for the western U.S. coniferous forest wildfires sampled during WE-CAN.

Overall, WE-CAN field observations greatly expand the number of measured VOC emission ratios and emission factors for wildfires, which provide better constraints on emissions in air quality models. Future studies of nighttime and early morning wildfire emissions would

complement the WE-CAN dataset. Additionally, more work connecting laboratory, ground, and aircraft observations would better inform how smoldering combustion emissions, not lofted into the main plume, may bias airborne measurements. We also have limited information about how early plume chemistry may impact comparisons between laboratory and field measured EFs for reactive VOCs and the total organic emissions.

**Acknowledgments**

The 2018 WE-CAN field campaign was supported by the U.S. National Science Foundation through grants # AGS-1650275 (U of Montana), -1650786 (Colorado State U), -1650288 (U of Colorado at Boulder), -1650493 (U of Wyoming), -1652688 (U of Washington), -1748266 (U of Montana), and National Oceanic and Atmospheric Administration (Award # NA17OAR4310010, Colorado State U). We thank Glenn Wolfe (NASA Goddard Space Flight Center/ University of Maryland Baltimore County) for his assistance in formaldehyde calibrations. This material is based upon work supported by the National Center for Atmospheric Research, which is a major facility sponsored by the National Science Foundation under Cooperative Agreement No. 1852977. The data were collected using NSF's Lower Atmosphere Observing Facilities, which are managed and operated by NCAR's Earth Observing Laboratory. All data are available in the WE-CAN data archive (https://data.eol.ucar.edu/master_lists/generated/we-can/).

## References


Akagi, S. K., Yokelson, R. J., Wiedinmyer, C., Alvarado, M. J., Reid, J. S., Karl, T., et al. (2011). Emission factors for open and domestic biomass burning for use in atmospheric models. *Atmospheric Chemistry and Physics*, *11*(9), 4039–4072. https://doi.org/10.5194/acp-11-4039-2011

Akagi, S. K., Craven, J. S., Taylor, J. W., McMeeking, G. R., Yokelson, R. J., Burling, I. R., et al. (2012). Evolution of trace gases and particles emitted by a chaparral fire in California. *Atmospheric Chemistry and Physics*, *12*(3), 1397–1421. https://doi.org/10.5194/acp-12-1397-2012

Akagi, S. K., Yokelson, R. J., Burling, I. R., Meinardi, S., Simpson, I., Blake, D. R., et al. (2013). Measurements of reactive trace gases and variable O3 formation rates in some South Carolina biomass burning plumes. *Atmospheric Chemistry and Physics*, *13*(3), 1141–1165. https://doi.org/10.5194/acp-13-1141-2013

Andreae, M. O., & Merlet, P. (2001). Emission of trace gases and aerosols from biomass burning. *Global Biogeochemical Cycles*, *15*(4), 955–966. https://doi.org/10.1029/2000GB001382

Andrews, S. J., Carpenter, L. J., Apel, E. C., Atlas, E., Donets, V., Hopkins, J. R., et al. (2016). A comparison of very short lived halocarbon (VSLS) and DMS aircraft measurements in the tropical west Pacific from CAST, ATTREX and CONTRAST. *Atmospheric Measurement Techniques*, *9*(10), 5213–5225. https://doi.org/10.5194/amt-9-5213-2016

Apel, E. C., Hills, A. J., Lueb, R., Zindel, S., Eisele, S., & Riemer, D. D. (2003). A fast-GC/MS system to measure C2 to C4 carbonyls and methanol aboard aircraft. *Journal of Geophysical Research: Atmospheres*, *108*(D20). https://doi.org/10.1029/2002JD003199

Apel, E. C., Emmons, L. K., Karl, T., Flocke, F., Hills, A. J., Madronich, S., et al. (2010). Chemical evolution of volatile organic compounds in the outflow of the Mexico City Metropolitan area. *Atmos. Chem. Phys.*, 23.

Apel, E. C., Hornbrook, R. S., Hills, A. J., Blake, N. J., Barth, M. C., Weinheimer, A., et al. (2015). Upper tropospheric ozone production from lightning NOx-impacted convection: Smoke ingestion case study from the DC3 campaign. *Journal of Geophysical Research: Atmospheres*, *120*(6), 2505–2523. https://doi.org/10.1002/2014JD022121

Baasandorj, M., Millet, D. B., Hu, L., Mitroo, D., & Williams, B. J. (2015). Measuring acetic and formic acid by proton-transfer-reaction mass spectrometry: sensitivity, humidity dependence, and quantifying interferences. *Atmospheric Measurement Techniques*, *8*(3), 1303–1321. https://doi.org/10.5194/amt-8-1303-2015

Baker, K. R., Woody, M. C., Tonnesen, G. S., Hutzell, W., Pye, H. O. T., Beaver, M. R., et al. (2016). Contribution of regional-scale fire events to ozone and PM2.5 air quality estimated by photochemical modeling approaches. *Atmospheric Environment*, *140*, 539–554. https://doi.org/10.1016/j.atmosenv.2016.06.032

Benedict, K. B., Zhou, Y., Sive, B. C., Prenni, A. J., Gebhart, K. A., Fischer, E. V., et al. (2019). Volatile organic compounds and ozone in Rocky Mountain National Park during FRAPPÉ. *Atmospheric Chemistry and Physics*, *19*(1), 499–521. https://doi.org/10.5194/acp-19-499-2019

Benedict, K. B., Prenni, A. J., El-Sayed, M. M. H., Hecobian, A., Zhou, Y., Gebhart, K. A., et al. (2020). Volatile organic compounds and ozone at four national parks in the southwestern United States. *Atmospheric Environment*, *239*, 117783. https://doi.org/10.1016/j.atmosenv.2020.117783

Bertschi, I., Yokelson, R. J., Ward, D. E., Babbitt, R. E., Susott, R. A., Goode, J. G., & Hao, W. M. (2003). Trace gas and particle emissions from fires in large diameter and belowground biomass fuels. *Journal of Geophysical Research: Atmospheres*, *108*(D13). https://doi.org/10.1029/2002JD002100

Bowman, D. M. J. S., Williamson, G. J., Abatzoglou, J. T., Kolden, C. A., Cochrane, M. A., & Smith, A. M. S. (2017). Human exposure and sensitivity to globally extreme wildfire events. *Nature Ecology & Evolution*, *1*(3), 0058. https://doi.org/10.1038/s41559-016-0058

Bruns, E. A., Slowik, J. G., El Haddad, I., Kilic, D., Klein, F., Dommen, J., et al. (2017). Characterization of gas-phase organics using proton transfer reaction time-of-flight mass spectrometry: fresh and aged residential wood combustion emissions. *Atmospheric Chemistry and Physics*, *17*(1), 705–720. https://doi.org/10.5194/acp-17-705-2017

Christian, T. J., Kleiss, B., Yokelson, R. J., Holzinger, R., Crutzen, P. J., Hao, W. M., et al. (2003). Comprehensive laboratory measurements of biomass-burning emissions: 1. Emissions from Indonesian, African, and other fuels. *Journal of Geophysical Research: Atmospheres*, *108*(D23). https://doi.org/10.1029/2003JD003704

Crutzen, P., & Andreae, M. (1991). Biomass Burning in the Tropics: Impact on Atmospheric Chemistry and Biogeochemical Cycles. *Science (New York, N.Y.)*, *250*, 1669–78. https://doi.org/10.1126/science.250.4988.1669

Ferek, R. J., Reid, J. S., Hobbs, P. V., Blake, D. R., & Liousse, C. (1998). Emission factors of hydrocarbons, halocarbons, trace gases and particles from biomass burning in Brazil. *Journal of Geophysical Research: Atmospheres*, *103*(D24), 32107–32118. https://doi.org/10.1029/98JD00692

1018 Garofalo, L. A., Pothier, M. A., Levin, E. J. T., Campos, T., Kreidenweis, S. M., & Farmer, D. K. (2019). Emission
1019 and Evolution of Submicron Organic Aerosol in Smoke from Wildfires in the Western United States. *ACS*
1020 *Earth and Space Chemistry*, *3*(7), 1237–1247. https://doi.org/10.1021/acsearthspacechem.9b00125
1021 Gilman, J. B., Lerner, B. M., Kuster, W. C., Goldan, P. D., Warneke, C., Veres, P. R., et al. (2015). Biomass burning
1022 emissions and potential air quality impacts of volatile organic compounds and other trace gases from fuels
1023 common in the US. *Atmospheric Chemistry and Physics*, *15*(24), 13915–13938. https://doi.org/10.5194/acp-
1024 15-13915-2015
1025 de Gouw, J. A., Goldan, P. D., Warneke, C., Kuster, W. C., Roberts, J. M., Marchewka, M., et al. (2003). Validation
1026 of proton transfer reaction-mass spectrometry (PTR-MS) measurements of gas-phase organic compounds in
1027 the atmosphere during the New England Air Quality Study (NEAQS) in 2002. *Journal of Geophysical*
1028 *Research: Atmospheres*, *108*(D21). https://doi.org/10.1029/2003JD003863
1029 Gueneron, M., Erickson, M. H., VanderSchelden, G. S., & Jobson, B. T. (2015). PTR-MS fragmentation patterns of
1030 gasoline hydrocarbons. *International Journal of Mass Spectrometry*, *379*, 97–109.
1031 https://doi.org/10.1016/j.ijms.2015.01.001
1032 Guérette, E.-A., Paton-Walsh, C., Desservettaz, M., Smith, T. E. L., Volkova, L., Weston, C. J., & Meyer, C. P. (2018).
1033 Emissions of trace gases from Australian temperate forest fires: emission factors and dependence on modified
1034 combustion efficiency. *Atmospheric Chemistry and Physics*, *18*(5), 3717–3735. https://doi.org/10.5194/acp-
1035 18-3717-2018
1036 Haase, K. B., Keene, W. C., Pszenny, A. A. P., Mayne, H. R., Talbot, R. W., & Sive, B. C. (2012). Calibration and
1037 intercomparison of acetic acid measurements using proton-transfer-reaction mass spectrometry (PTR-MS).
1038 *Atmospheric Measurement Techniques*, *5*(11), 2739–2750. https://doi.org/10.5194/amt-5-2739-2012
1039 Hatch, L. E., Yokelson, R. J., Stockwell, C. E., Veres, P. R., Simpson, I. J., Blake, D. R., et al. (2017). Multi-instrument
1040 comparison and compilation of non-methane organic gas emissions from biomass burning and implications
1041 for smoke-derived secondary organic aerosol precursors. *Atmospheric Chemistry and Physics*, *17*(2), 1471–
1042 1489. https://doi.org/10.5194/acp-17-1471-2017
1043 Hatch, L. E., Jen, C. N., Kreisberg, N. M., Selimovic, V., Yokelson, R. J., Stamatis, C., et al. (2019). Highly Speciated
1044 Measurements of Terpenoids Emitted from Laboratory and Mixed-Conifer Forest Prescribed Fires.
1045 *Environmental Science & Technology*, *53*(16), 9418–9428. https://doi.org/10.1021/acs.est.9b02612

1046 Hobbs, P. V., Sinha, P., Yokelson, R. J., Christian, T. J., Blake, D. R., Gao, S., et al. (2003). Evolution of gases and
1047 particles from a savanna fire in South Africa. *Journal of Geophysical Research: Atmospheres*, *108*(D13).
1048 https://doi.org/10.1029/2002JD002352
1049 Holder, A. L., Gullett, B. K., Urbanski, S. P., Elleman, R., O'Neill, S., Tabor, D., et al. (2017). Emissions from
1050 prescribed burning of agricultural fields in the Pacific Northwest. *Atmospheric Environment*, *166*, 22–33.
1051 https://doi.org/10.1016/j.atmosenv.2017.06.043
1052 Hornbrook, R. S., Blake, D. R., Diskin, G. S., Fried, A., Fuelberg, H. E., Meinardi, S., et al. (2011). Observations of
1053 nonmethane organic compounds during ARCTAS − Part 1: Biomass burning emissions and plume
1054 enhancements. *Atmospheric Chemistry and Physics*, *11*(21), 11103–11130. https://doi.org/10.5194/acp-11-
1055 11103-2011
1056 Jolly, W. (2015). Climate-induced variations in global wildfire danger from 1979 to 2013. *Nature Communications*,
1057 *6*, 7537. https://doi.org/10.1038/ncomms8537
1058 Karl, T., Hansel, A., Cappellin, L., Kaser, L., Herdlinger-Blatt, I., & Jud, W. (2012). Selective measurements of
1059 isoprene and 2-methyl-3-buten-2-ol based on $NO^+$ ionization mass spectrometry. *Atmospheric Chemistry*
1060 *and Physics*, *12*(24), 11877–11884. https://doi.org/10.5194/acp-12-11877-2012
1061 Koss, A. R., Sekimoto, K., Gilman, J. B., Selimovic, V., Coggon, M. M., Zarzana, K. J., et al. (2018). Non-methane
1062 organic gas emissions from biomass burning: identification, quantification, and emission factors from PTR-
1063 ToF during the FIREX 2016 laboratory experiment. *Atmospheric Chemistry and Physics*, *18*(5), 3299–3319.
1064 https://doi.org/10.5194/acp-18-3299-2018
1065 Larkin, N. K., Raffuse, S. M., & Strand, T. M. (2014). Wildland fire emissions, carbon, and climate: U.S. emissions
1066 inventories. *Wildland Fire Emissions, Carbon, and Climate: Science Overview and Knowledge Needs*, *317*,
1067 61–69. https://doi.org/10.1016/j.foreco.2013.09.012
1068 Lee, B. H., Lopez-Hilfiker, F. D., Mohr, C., Kurtén, T., Worsnop, D. R., & Thornton, J. A. (2014). An Iodide-Adduct
1069 High-Resolution Time-of-Flight Chemical-Ionization Mass Spectrometer: Application to Atmospheric
1070 Inorganic and Organic Compounds. *Environmental Science & Technology*, *48*(11), 6309–6317.
1071 https://doi.org/10.1021/es500362a
1072 Liu, X., Huey, L. G., Yokelson, R. J., Selimovic, V., Simpson, I. J., Müller, M., et al. (2017). Airborne measurements
1073 of western U.S. wildfire emissions: Comparison with prescribed burning and air quality implications:

1074 Western U.S. Wildfire Emissions. *Journal of Geophysical Research: Atmospheres*, *122*(11), 6108–6129.
1075 https://doi.org/10.1002/2016JD026315
1076 McClure, C. D., & Jaffe, D. A. (2018). US particulate matter air quality improves except in wildfire-prone areas.
1077 *Proceedings of the National Academy of Sciences*, *115*(31), 7901–7906.
1078 https://doi.org/10.1073/pnas.1804353115
1079 Müller, M., Anderson, B. E., Beyersdorf, A. J., Crawford, J. H., Diskin, G. S., Eichler, P., et al. (2016). In situ
1080 measurements and modeling of reactive trace gases in a small biomass burning plume. *Atmospheric*
1081 *Chemistry and Physics*, *16*(6), 3813–3824. https://doi.org/10.5194/acp-16-3813-2016
1082 O'Dell, K., Ford, B., Fischer, E. V., & Pierce, J. R. (2019). Contribution of Wildland-Fire Smoke to US PM2.5 and
1083 Its Influence on Recent Trends. *Environmental Science & Technology*, *53*(4), 1797–1804.
1084 https://doi.org/10.1021/acs.est.8b05430
1085 Ottmar, R. D. (2014). Wildland fire emissions, carbon, and climate: Modeling fuel consumption. *Wildland Fire*
1086 *Emissions, Carbon, and Climate: Science Overview and Knowledge Needs*, *317*, 41–50.
1087 https://doi.org/10.1016/j.foreco.2013.06.010
1088 Pagonis, D., Sekimoto, K., & de Gouw, J. (2019). A Library of Proton-Transfer Reactions of H3O+ Ions Used for
1089 Trace Gas Detection. *Journal of The American Society for Mass Spectrometry*, *30*(7), 1330–1335.
1090 https://doi.org/10.1007/s13361-019-02209-3
1091 Palm, B. B., Liu, X., Jimenez, J. L., & Thornton, J. A. (2019). Performance of a new coaxial ion–molecule reaction
1092 region for low-pressure chemical ionization mass spectrometry with reduced instrument wall interactions.
1093 *Atmospheric Measurement Techniques*, *12*(11), 5829–5844. https://doi.org/10.5194/amt-12-5829-2019
1094 Peng, Q., Palm, B. B., Melander, K. E., Lee, B. H., Hall, S. R., Ullmann, K., et al. (2020). HONO Emissions from
1095 Western U.S. Wildfires Provide Dominant Radical Source in Fresh Wildfire Smoke. *Environmental Science*
1096 *& Technology*, *54*(10), 5954–5963. https://doi.org/10.1021/acs.est.0c00126
1097 Prichard, S. J., O'Neill, S. M., Eagle, P., Andreu, A. G., Drye, B., Dubowy, J., et al. (2020). Wildland fire emission
1098 factors in North America: synthesis of existing data, measurement needs and management applications.
1099 *International Journal of Wildland Fire*, *29*(2), 132. https://doi.org/10.1071/WF19066
1100 R Core Team. (2019). *R: A Language and Environment for Statistical Computing*. Vienna, Austria: R Foundation for
1101 Statistical Computing. Retrieved from https://www.R-project.org/

1102 Roberts, J. M., Stockwell, C. E., Yokelson, R. J., de Gouw, J., Liu, Y., Selimovic, V., et al. (2020). The nitrogen
1103 budget of laboratory-simulated western U.S. wildfires during the FIREX 2016 FireLab study. *Atmospheric*
1104 *Chemistry and Physics Discussions*, *2020*, 1–34. https://doi.org/10.5194/acp-2020-66
1105 RStudio Team. (2020). *RStudio: Integrated Development Environment for R*. Boston, MA: RStudio, PBC. Retrieved
1106 from http://www.rstudio.com/
1107 Russo, R. S., Zhou, Y., White, M. L., Mao, H., Talbot, R., & Sive, B. C. (2010). Multi-year (2004–2008) record of
1108 nonmethane hydrocarbons and halocarbons in New England: seasonal variations and regional sources.
1109 *Atmospheric Chemistry and Physics*, *10*(10), 4909–4929. https://doi.org/10.5194/acp-10-4909-2010
1110 Santín, C., Doerr, S. H., Preston, C. M., & González-Rodríguez, G. (2015). Pyrogenic organic matter production from
1111 wildfires: a missing sink in the global carbon cycle. *Global Change Biology*, *21*(4), 1621–1633.
1112 https://doi.org/10.1111/gcb.12800
1113 Schwarz, J. P., Gao, R. S., Spackman, J. R., Watts, L. A., Thomson, D. S., Fahey, D. W., et al. (2008). Measurement
1114 of the mixing state, mass, and optical size of individual black carbon particles in urban and biomass burning
1115 emissions. *Geophysical Research Letters*, *35*(13). https://doi.org/10.1029/2008GL033968
1116 Sekimoto, K., Li, S.-M., Yuan, B., Koss, A., Coggon, M., Warneke, C., & de Gouw, J. (2017). Calculation of the
1117 sensitivity of proton-transfer-reaction mass spectrometry (PTR-MS) for organic trace gases using molecular
1118 properties. *International Journal of Mass Spectrometry*, *421*, 71–94.
1119 https://doi.org/10.1016/j.ijms.2017.04.006
1120 Sekimoto, K., Koss, A. R., Gilman, J. B., Selimovic, V., Coggon, M. M., Zarzana, K. J., et al. (2018). High- and low-
1121 temperature pyrolysis profiles describe volatile organic compound emissions from western US wildfire fuels.
1122 *Atmospheric Chemistry and Physics*, *18*(13), 9263–9281. https://doi.org/10.5194/acp-18-9263-2018
1123 Selimovic, V., Yokelson, R. J., Warneke, C., Roberts, J. M., de Gouw, J., Reardon, J., & Griffith, D. W. T. (2018).
1124 Aerosol optical properties and trace gas emissions by PAX and OP-FTIR for laboratory-simulated western
1125 US wildfires during FIREX. *Atmospheric Chemistry and Physics*, *18*(4), 2929–2948.
1126 https://doi.org/10.5194/acp-18-2929-2018
1127 Selimovic, V., Yokelson, R. J., McMeeking, G. R., & Coefield, S. (2019). In situ measurements of trace gases, PM,
1128 and aerosol optical properties during the 2017 NW US wildfire smoke event. *Atmospheric Chemistry and*
1129 *Physics*, *19*(6), 3905–3926. https://doi.org/10.5194/acp-19-3905-2019

1130 Stockwell, C. E., Yokelson, R. J., Kreidenweis, S. M., Robinson, A. L., DeMott, P. J., Sullivan, R. C., et al. (2014).
1131 Trace gas emissions from combustion of peat, crop residue, domestic biofuels, grasses, and other fuels:
1132 configuration and Fourier transform infrared (FTIR) component of the fourth Fire Lab at Missoula
1133 Experiment (FLAME-4). *Atmospheric Chemistry and Physics*, *14*(18), 9727–9754.
1134 https://doi.org/10.5194/acp-14-9727-2014
1135 Stockwell, C. E., Veres, P. R., Williams, J., & Yokelson, R. J. (2015). Characterization of biomass burning emissions
1136 from cooking fires, peat, crop residue, and other fuels with high-resolution proton-transfer-reaction time-of-
1137 flight mass spectrometry. *Atmospheric Chemistry and Physics*, *15*(2), 845–865. https://doi.org/10.5194/acp-
1138 15-845-2015
1139 Urbanski, S. (2014). Wildland fire emissions, carbon, and climate: Emission factors. *Forest Ecology and Management*,
1140 *317*, 51–60. https://doi.org/10.1016/j.foreco.2013.05.045
1141 U.S. Environmental Protection Agency. (2020). 2017 National Emissions Inventory (NEI) Technical Support
1142 Document (TSD). Retrieved from https://www.epa.gov/sites/production/files/2020-
1143 04/documents/nei2017_tsd_full_30apr2020.pdf
1144 Veres, P., Gilman, J. B., Roberts, J. M., Kuster, W. C., Warneke, C., Burling, I. R., & de Gouw, J. (2010). Development
1145 and validation of a portable gas phase standard generation and calibration system for volatile organic
1146 compounds. *Atmospheric Measurement Techniques*, *3*(3), 683–691. https://doi.org/10.5194/amt-3-683-2010
1147 Vlasenko, A., Macdonald, A. . M., Sjostedt, S. J., & Abbatt, J. P. D. (2010). Formaldehyde measurements by Proton
1148 transfer reaction – Mass Spectrometry (PTR-MS): correction for humidity effects. *Atmospheric Measurement*
1149 *Techniques*, *3*(4), 1055–1062. https://doi.org/10.5194/amt-3-1055-2010
1150 Warneke, C., Veres, P., Holloway, J. S., Stutz, J., Tsai, C., Alvarez, S., et al. (2011). Airborne formaldehyde
1151 measurements using PTR-MS: calibration, humidity dependence, inter-comparison and initial results.
1152 *Atmospheric Measurement Techniques*, *4*(10), 2345–2358. https://doi.org/10.5194/amt-4-2345-2011
1153 van der Werf, G. R., Randerson, J. T., Giglio, L., van Leeuwen, T. T., Chen, Y., Rogers, B. M., et al. (2017). Global
1154 fire emissions estimates during 1997–2016. *Earth System Science Data*, *9*(2), 697–720.
1155 https://doi.org/10.5194/essd-9-697-2017
1156 Westerling, A. L. (2006). Warming and Earlier Spring Increase Western U.S. Forest Wildfire Activity. *Science*,
1157 *313*(5789), 940–943. https://doi.org/10.1126/science.1128834

1158 Westerling, A. L. (2016). Increasing western US forest wildfire activity: sensitivity to changes in the timing of spring.
1159 *Philosophical Transactions of the Royal Society B: Biological Sciences*, *371*(1696), 20150178.
1160 https://doi.org/10.1098/rstb.2015.0178
1161 Wickham, H. (2016). *ggplot2: Elegant Graphics for Data Analysis*. Springer-Verlag New York. Retrieved from
1162 https://ggplot2.tidyverse.org
1163 Wickham, H., François, R., Henry, L., & Müller, K. (2019). *dplyr: A Grammar of Data Manipulation*. Retrieved from
1164 https://CRAN.R-project.org/package=dplyr
1165 Wiedinmyer, C., Akagi, S. K., Yokelson, R. J., Emmons, L. K., Al-Saadi, J. A., Orlando, J. J., & Soja, A. J. (2011).
1166 The Fire INventory from NCAR (FINN): a high resolution global model to estimate the emissions from open
1167 burning. *Geoscientific Model Development*, *4*(3), 625–641. https://doi.org/10.5194/gmd-4-625-2011
1168 Yokelson, R. J., Griffith, D. W. T., & Ward, D. E. (1996). Open-path Fourier transform infrared studies of large-scale
1169 laboratory biomass fires. *Journal of Geophysical Research: Atmospheres*, *101*(D15), 21067–21080.
1170 https://doi.org/10.1029/96JD01800
1171 Yokelson, R. J., Goode, J. G., Ward, D. E., Susott, R. A., Babbitt, R. E., Wade, D. D., et al. (1999). Emissions of
1172 formaldehyde, acetic acid, methanol, and other trace gases from biomass fires in North Carolina measured
1173 by airborne Fourier transform infrared spectroscopy. *Journal of Geophysical Research: Atmospheres*,
1174 *104*(D23), 30109–30125. https://doi.org/10.1029/1999JD900817
1175 Yokelson, R. J., Christian, T. J., Karl, T. G., & Guenther, A. (2008). The tropical forest and fire emissions experiment:
1176 laboratory fire measurements and synthesis of campaign data. *Atmos. Chem. Phys.*, 19.
1177 Yokelson, R. J., Burling, I. R., Gilman, J. B., Warneke, C., Stockwell, C. E., de Gouw, J., et al. (2013). Coupling field
1178 and laboratory measurements to estimate the emission factors of identified and unidentified trace gases for
1179 prescribed fires. *Atmospheric Chemistry and Physics*, *13*(1), 89–116. https://doi.org/10.5194/acp-13-89-2013
1180 Yuan, B., Warneke, C., Shao, M., & de Gouw, J. A. (2014). Interpretation of volatile organic compound measurements
1181 by proton-transfer-reaction mass spectrometry over the deepwater horizon oil spill. *International Journal of*
1182 *Mass Spectrometry*, *358*, 43–48. https://doi.org/10.1016/j.ijms.2013.11.006
1183 Yuan, B., Koss, A. R., Warneke, C., Coggon, M., Sekimoto, K., & de Gouw, J. A. (2017). Proton-Transfer-Reaction
1184 Mass Spectrometry: Applications in Atmospheric Sciences. *Chemical Reviews*, *117*(21), 13187–13229.
1185 https://doi.org/10.1021/acs.chemrev.7b00325

1186 Zhou, Y., Shively, D., Mao, H., Russo, R. S., Pape, B., Mower, R. N., et al. (2010). Air Toxic Emissions from
1187 Snowmobiles in Yellowstone National Park. *Environmental Science & Technology*, *44*(1), 222–228.
1188 https://doi.org/10.1021/es9018578

1189

1190

1191

1192

1193

1194 **Table 2.** *WE-CAN Campaign-averaged Emission Ratios, Emission Factors, and VOC Mass*
1195 *Fractions.*

| VOC contributor[a] | Exact mass[b], Da | Chemical formula | N[c] | ER to CO, ppb ppm$^{-1}$ (σ) | EF, g kg$^{-1}$ (σ) | VOC mass fraction % |
|---|---|---|---|---|---|---|
| *Carbon dioxide* | 43.99 | $CO_2$ | 24 | 9520.00 (2500.00) | 1413.00 (61.00) | - |
| *Carbon monoxide* | 27.995 | CO | 24 | 1000.00 (-) | 99.30 (20.00) | - |
| *Methane* | 16.031 | $CH_4$ | 24 | 102.00 (17.00) | 5.93 (1.80) | - |
| Ethyne[e] | 26.016 | $C_2H_2$ | 16 | 3.50 (1.80) | 0.31 (0.17) | 1.20 (0.71) |
| Hydrogen cyanide[d] | 27.011 | HCN | 15 | 4.30 (1.70) | 0.43 (0.17) | 1.70 (0.79) |
| Ethene[e] | 28.031 | $C_2H_4$ | 16 | 16.00 (9.10) | 1.50 (1.00) | 5.90 (4.20) |
| Formaldehyde | 30.011 | $CH_2O$ | 24 | 18.00 (3.30) | 1.90 (0.43) | 7.30 (2.50) |
| Ethane[e] | 30.047 | $C_2H_6$ | 16 | 10.00 (6.70) | 1.10 (0.84) | 4.30 (3.40) |
| Methanol | 32.026 | $CH_4O$ | 24 | 13.00 (2.00) | 1.50 (0.39) | 5.80 (2.10) |
| Acetonitrile | 41.027 | $C_2H_3N$ | 24 | 2.10 (0.99) | 0.31 (0.15) | 1.20 (0.65) |
| Propene[e] | 42.047 | $C_3H_6$ | 16 | 4.90 (3.60) | 0.74 (0.62) | 2.90 (2.50) |
| Isocyanic acid | 43.006 | HNCO | 24 | 1.10 (0.35) | 0.16 (0.036) | 0.61 (0.21) |
| Ethenamine | 43.042 | $C_2H_5N$ | 24 | 0.072 (0.034) | 0.011 (0.0058) | 0.043 (0.025) |
| Acetaldehyde | 44.026 | $C_2H_4O$ | 24 | 11.00 (1.60) | 1.70 (0.43) | 6.30 (2.30) |
| Propane[d] | 44.063 | $C_3H_8$ | 15 | 2.70 (0.92) | 0.46 (0.18) | 1.80 (0.84) |
| Formamide | 45.021 | $CH_3NO$ | 24 | 0.23 (0.08) | 0.037 (0.014) | 0.14 (0.066) |
| Formic acid[f] | 46.005 | $CH_2O_2$ | 20 | 9.50 (4.20) | 1.50 (0.60) | 5.70 (2.70) |
| Ethanol[d] | 46.042 | $C_2H_6O$ | 13 | 0.19 (0.17) | 0.035 (0.04) | 0.13 (0.16) |
| Methyl chloride[d] | 49.992 | $CH_3Cl$ | 15 | 0.092 (0.047) | 0.017 (0.0089) | 0.067 (0.038) |
| 1-Buten-3-yne | 52.031 | $C_4H_4$ | 24 | 0.28 (0.088) | 0.052 (0.018) | 0.20 (0.087) |
| Acrylonitrile | 53.027 | $C_3H_3N$ | 24 | 0.23 (0.076) | 0.044 (0.015) | 0.17 (0.074) |
| 2-Propynal | 54.011 | $C_3H_2O$ | 24 | 0.20 (0.089) | 0.037 (0.015) | 0.14 (0.07) |
| 1,3-Butadiene, 1,2-Butadiene | 54.047 | $C_4H_6$ | 24 | 1.40 (0.38) | 0.27 (0.096) | 1.00 (0.46) |
| Propanenitrile | 55.042 | $C_3H_5N$ | 24 | 0.19 (0.087) | 0.037 (0.018) | 0.14 (0.077) |
| Acrolein[d] | 56.026 | $C_3H_4O$ | 15 | 1.90 (0.66) | 0.40 (0.18) | 1.50 (0.79) |
| Butenes | 56.063 | $C_4H_8$ | 24 | 1.30 (0.52) | 0.26 (0.12) | 1.00 (0.52) |

| | | | | | | |
|---|---|---|---|---|---|---|
| *Isobutene, 1-Butene*[d] | 56.063 | $C_4H_8$ | 15 | 1.30 (0.78) | 0.28 (0.17) | - |
| Methyl isocyanate, Hydroxyacetonitrile | 57.021 | $C_2H_3NO$ | 24 | 0.16 (0.03) | 0.033 (0.0087) | 0.13 (0.047) |
| Propeneamines | 57.058 | $C_3H_7N$ | 24 | 0.087 (0.035) | 0.018 (0.0082) | 0.07 (0.037) |
| Glyoxal | 58.005 | $C_2H_2O_2$ | 22 | 0.028 (0.023) | 0.0054 (0.0045) | 0.021 (0.018) |
| Acetone, Propanal | 58.042 | $C_3H_6O$ | 24 | 4.10 (0.64) | 0.84 (0.22) | 3.20 (1.20) |
| *Acetone*[d] | 58.042 | $C_3H_6O$ | 15 | 2.90 (1.40) | 0.65 (0.38) | - |
| *Propanal*[d] | 58.042 | $C_3H_6O$ | 15 | 0.81 (0.30) | 0.18 (0.07) | - |
| n-Butane[d] | 58.078 | $C_4H_{10}$ | 15 | 0.56 (0.26) | 0.12 (0.061) | 0.48 (0.27) |
| Isobutane[d] | 58.078 | $C_4H_{10}$ | 15 | 0.17 (0.088) | 0.038 (0.019) | 0.14 (0.084) |
| Acetamide | 59.037 | $C_2H_5NO$ | 24 | 0.19 (0.046) | 0.04 (0.012) | 0.15 (0.061) |
| Trimethylamine | 59.073 | $C_3H_9N$ | 24 | 0.026 (0.0085) | 0.0054 (0.002) | 0.021 (0.0095) |
| Acetic acid, glycolaldehyde (=hydroxyacetaldehyde) | 60.021 | $C_2H_4O_2$ | 24 | 11.00 (2.10) | 2.40 (0.61) | 9.40 (3.40) |
| Isopropanol[d] | 60.058 | $C_3H_8O$ | 14 | 0.032 (0.021) | 0.0074 (0.0058) | 0.028 (0.024) |
| Nitromethane | 61.016 | $CH_3NO_2$ | 24 | 0.38 (0.10) | 0.078 (0.0085) | 0.30 (0.085) |
| Dimethyl sulfide[e] | 62.019 | $C_2H_6S$ | 9 | 0.41 (0.37) | 0.08 (0.083) | 0.31 (0.33) |
| Cyanoallene isomers | 65.027 | $C_4H_3N$ | 24 | 0.0074 (0.0055) | 0.0017 (0.0012) | 0.0064 (0.0049) |
| 1,3-Cyclopentadiene | 66.047 | $C_5H_6$ | 24 | 0.048 (0.018) | 0.011 (0.0049) | 0.044 (0.022) |
| Pyrrole, Butenenitrile isomers | 67.042 | $C_4H_5N$ | 24 | 0.16 (0.091) | 0.039 (0.021) | 0.15 (0.089) |
| *Methacrylonitrile*[d] | 67.042 | $C_4H_5N$ | 15 | 0.056 (0.043) | 0.014 (0.011) | - |
| Carbon suboxide | 67.99 | $C_3O_2$ | 21 | 0.037 (0.024) | 0.0084 (0.0054) | 0.032 (0.023) |
| Furan | 68.026 | $C_4H_4O$ | 24 | 1.70 (0.60) | 0.43 (0.19) | 1.70 (0.85) |
| Isoprene[d] | 68.063 | $C_5H_8$ | 15 | 0.31 (0.39) | 0.082 (0.095) | 0.31 (0.37) |
| Butanenitriles, Dihydropyrrole | 69.058 | $C_4H_7N$ | 24 | 0.081 (0.04) | 0.02 (0.01) | 0.077 (0.044) |
| Propiolic acid | 70.005 | $C_3H_2O_2$ | 23 | 0.044 (0.029) | 0.011 (0.0071) | 0.041 (0.029) |
| Methyl vinyl ketone, Methacrolein, 2-Butenal (=crotonaldehyde) | 70.042 | $C_4H_6O$ | 24 | 1.60 (0.51) | 0.39 (0.15) | 1.50 (0.71) |
| *Methyl vinyl ketone*[d] | 70.042 | $C_4H_6O$ | 15 | 0.75 (0.45) | 0.20 (0.12) | - |
| *Methacrolein*[d] | 70.042 | $C_4H_6O$ | 15 | 0.37 (0.26) | 0.097 (0.067) | - |
| *2-Butenal*[d] | 70.042 | $C_4H_6O$ | 15 | 0.15 (0.075) | 0.041 (0.02) | - |
| Pentenes & methylbutenes | 70.078 | $C_5H_{10}$ | 24 | 0.06 (0.03) | 0.015 (0.0084) | 0.059 (0.036) |
| *Cyclopentane*[e] | 70.078 | $C_5H_{10}$ | 16 | 0.014 (0.0088) | 0.0035 (0.0025) | - |
| Buteneamines, tetrahydropyrrole | 71.073 | $C_4H_9N$ | 21 | 0.014 (0.011) | 0.0036 (0.003) | 0.014 (0.012) |
| Pyruvaldehyde (=methyl glyoxal), Acrylic acid | 72.021 | $C_3H_4O_2$ | 24 | 0.84 (0.26) | 0.22 (0.082) | 0.83 (0.39) |
| Methyl ethyl ketone, 2-Methylpropanal, Butanal | 72.058 | $C_4H_8O$ | 24 | 0.82 (0.17) | 0.21 (0.063) | 0.81 (0.32) |
| *Methyl ethyl ketone*[d] | 72.058 | $C_4H_8O$ | 15 | 0.73 (0.27) | 0.20 (0.075) | - |
| *Butanal*[d] | 72.058 | $C_4H_8O$ | 15 | 0.19 (0.079) | 0.053 (0.023) | - |
| n-Pentane[d] | 72.094 | $C_5H_{12}$ | 15 | 0.21 (0.094) | 0.057 (0.028) | 0.22 (0.12) |
| Isopentane[d] | 72.094 | $C_5H_{12}$ | 15 | 0.069 (0.043) | 0.019 (0.012) | 0.073 (0.05) |
| Nitroethene | 73.016 | $C_2H_3NO_2$ | 24 | 0.038 (0.013) | 0.0099 (0.0037) | 0.038 (0.017) |
| Hydroxyacetone, Methyl acetate, Ethyl formate | 74.037 | $C_3H_6O_2$ | 24 | 2.10 (0.57) | 0.57 (0.20) | 2.20 (0.97) |
| Nitroethane, ethyl nitrite | 75.032 | $C_2H_5NO_2$ | 24 | 0.045 (0.012) | 0.012 (0.0042) | 0.047 (0.02) |
| Carbon disulfide[d] | 75.944 | $CS_2$ | 15 | 0.0016 (0.0012) | 4.5e-04 (3.1e-04) | 0.0017 (0.0013) |
| Benzene | 78.047 | $C_6H_6$ | 24 | 1.80 (0.24) | 0.50 (0.14) | 1.90 (0.73) |

| | | | | | | |
|---|---|---|---|---|---|---|
| Pentadienenitriles, Pyridine | 79.042 | $C_5H_5N$ | 24 | 0.13 (0.025) | 0.037 (0.01) | 0.14 (0.055) |
| 2,4-Cyclopentadiene-1-one | 80.026 | $C_5H_4O$ | 24 | 0.092 (0.052) | 0.027 (0.017) | 0.11 (0.07) |
| Pentenenitriles, Methylpyrroles | 81.058 | $C_5H_7N$ | 24 | 0.069 (0.039) | 0.02 (0.011) | 0.077 (0.048) |
| 2-Methylfuran, 3-Methylfuran | 82.042 | $C_5H_6O$ | 24 | 0.92 (0.38) | 0.28 (0.13) | 1.10 (0.58) |
| *2-Methylfuran*[d] | 82.042 | $C_5H_6O$ | 12 | 0.15 (0.09) | 0.047 (0.03) | - |
| *3-Methylfuran*[d] | 82.042 | $C_5H_6O$ | 14 | 0.03 (0.021) | 0.0097 (0.0071) | - |
| 2,2-Dimethylbutane[e] | 82.078 | $C_6H_{10}$ | 14 | 0.055 (0.037) | 0.015 (0.011) | 0.058 (0.043) |
| Pentanenitriles | 83.073 | $C_5H_9N$ | 24 | 0.071 (0.037) | 0.021 (0.011) | 0.08 (0.047) |
| Dichloromethane[d] | 83.953 | $CH_2Cl_2$ | 14 | 0.0088 (0.0064) | 0.0029 (0.0022) | 0.011 (0.009) |
| 2(3H)-Furanone | 84.021 | $C_4H_4O_2$ | 24 | 1.10 (0.28) | 0.32 (0.11) | 1.20 (0.54) |
| 3-Methyl-3-buten-2-one, Cyclopentanone | 84.058 | $C_5H_8O$ | 24 | 0.28 (0.099) | 0.087 (0.038) | 0.33 (0.17) |
| Cyclohexane[e] | 84.094 | $C_6H_{12}$ | 6 | 0.026 (0.043) | 0.008 (0.014) | 0.031 (0.055) |
| 2,3-Butanedione, Methyl acrylate | 86.037 | $C_4H_6O_2$ | 24 | 1.70 (0.52) | 0.53 (0.21) | 2.00 (0.97) |
| 3-Methyl-2-butanone, 2-Pentanone, 3-Pentanone, 2-Methylbutanal, 3-Methylbutanal | 86.073 | $C_5H_{10}O$ | 24 | 0.20 (0.058) | 0.062 (0.023) | 0.24 (0.11) |
| *2-Methyl-3-buten-2-ol*[d] | 86.073 | $C_5H_{10}O$ | 13 | 0.018 (0.01) | 0.0061 (0.0036) | - |
| n-Hexane[e] | 86.11 | $C_6H_{14}$ | 15 | 0.13 (0.10) | 0.04 (0.036) | 0.15 (0.14) |
| 3-Methylpentane[e] | 86.11 | $C_6H_{14}$ | 12 | 0.034 (0.019) | 0.01 (0.0065) | 0.039 (0.027) |
| Pyruvic acid | 88.016 | $C_3H_4O_3$ | 22 | 0.063 (0.026) | 0.019 (0.008) | 0.074 (0.036) |
| Methyl propanoate | 88.052 | $C_4H_8O_2$ | 24 | 0.25 (0.094) | 0.081 (0.036) | 0.31 (0.16) |
| Nitropropanes | 89.048 | $C_3H_7NO_2$ | 23 | 0.0074 (0.0033) | 0.0024 (0.0012) | 0.0092 (0.0052) |
| 2,4-Dimethylpentane[e] | 90.047 | $C_7H_{16}$ | 7 | 0.0076 (0.0094) | 0.0023 (0.003) | 0.0086 (0.012) |
| Ethylnylpyrrole | 91.042 | $C_6H_5N$ | 24 | 0.028 (0.0068) | 0.0091 (0.0026) | 0.035 (0.014) |
| Toluene | 92.063 | $C_7H_8$ | 24 | 1.20 (0.33) | 0.42 (0.16) | 1.60 (0.74) |
| 3-Furancarbonitrile, 2-Furancarbonitrile | 93.021 | $C_5H_3NO$ | 24 | 0.026 (0.0087) | 0.0088 (0.0037) | 0.034 (0.017) |
| 2-Methylpyridine, 3-Methylpyridine | 93.058 | $C_6H_7N$ | 24 | 0.10 (0.026) | 0.035 (0.012) | 0.13 (0.057) |
| Methyl bromide[d] | 93.942 | $CH_3Br$ | 14 | 0.0029 (0.002) | 1e-03 (7.1e-04) | 0.0039 (0.0029) |
| Phenol | 94.042 | $C_6H_6O$ | 24 | 0.98 (0.34) | 0.33 (0.13) | 1.30 (0.60) |
| 2-Furfural (=furaldehyde), 3-Furfural | 96.021 | $C_5H_4O_2$ | 24 | 1.50 (0.44) | 0.53 (0.21) | 2.00 (0.97) |
| C2-substituted furan isomers, 2,5-Dimethylfuran, 2-Ethylfuran | 96.058 | $C_6H_8O$ | 24 | 0.57 (0.25) | 0.20 (0.096) | 0.77 (0.42) |
| 4-methylpentanenitrile | 97.089 | $C_6H_{11}N$ | 24 | 0.025 (0.014) | 0.0088 (0.0047) | 0.034 (0.02) |
| 1,2-Dichloroethane[d] | 97.969 | $C_2H_4Cl_2$ | 10 | 0.002 (0.0022) | 8.2e-04 (9.1e-04) | 0.0032 (0.0036) |
| Maleic anhydride | 98 | $C_4H_2O_3$ | 24 | 0.44 (0.28) | 0.14 (0.072) | 0.55 (0.31) |
| 2-Furanmethanol | 98.037 | $C_5H_6O_2$ | 24 | 0.25 (0.10) | 0.09 (0.043) | 0.34 (0.19) |
| C6H10O ketones, Methylcyclopentanone, Cyclohexanone | 98.073 | $C_6H_{10}O$ | 24 | 0.096 (0.033) | 0.034 (0.015) | 0.13 (0.066) |
| Methylcyclohexane[e] | 98.11 | $C_7H_{14}$ | 13 | 0.05 (0.059) | 0.018 (0.022) | 0.07 (0.088) |
| Dihydrofurandione | 100.016 | $C_4H_4O_3$ | 23 | 0.16 (0.059) | 0.055 (0.019) | 0.21 (0.092) |
| Methyl methacrylate | 100.052 | $C_5H_8O_2$ | 24 | 0.31 (0.098) | 0.11 (0.045) | 0.44 (0.21) |
| Hexanones, Hexanal | 100.089 | $C_6H_{12}O$ | 23 | 0.036 (0.011) | 0.013 (0.0056) | 0.05 (0.025) |
| n-Heptane[e] | 100.125 | $C_7H_{16}$ | 16 | 0.13 (0.13) | 0.046 (0.05) | 0.18 (0.20) |
| 2-Methylhexane[e] | 100.125 | $C_7H_{16}$ | 9 | 0.057 (0.11) | 0.021 (0.042) | 0.079 (0.16) |

| | | | | | | |
|---|---|---|---|---|---|---|
| 3-Methylhexane[e] | 100.125 | $C_7H_{16}$ | 5 | 0.04 (0.046) | 0.016 (0.018) | 0.06 (0.072) |
| 2,3-Dimethylpentane[e] | 100.125 | $C_7H_{16}$ | 10 | 0.011 (0.019) | 0.0039 (0.0075) | 0.015 (0.029) |
| Acetic anhydride | 102.032 | $C_4H_6O_3$ | 24 | 0.12 (0.04) | 0.044 (0.02) | 0.17 (0.088) |
| Benzonitrile | 103.042 | $C_7H_5N$ | 24 | 0.15 (0.053) | 0.055 (0.022) | 0.21 (0.10) |
| Styrene[d] | 104.063 | $C_8H_8$ | 15 | 0.045 (0.028) | 0.018 (0.012) | 0.07 (0.048) |
| Isopropyl nitrate[d] | 105.043 | $C_3H_7NO_3$ | 13 | 0.0033 (0.0014) | 0.0013 (5.5e-04) | 0.0049 (0.0025) |
| n-propyl nitrate | 105.043 | $C_3H_7NO_3$ | 4 | 0.0015 (6.5e-04) | 5.3e-04 (2.4e-04) | 0.002 (0.0011) |
| Vinylpyridine | 105.058 | $C_7H_7N$ | 24 | 0.022 (0.0092) | 0.0085 (0.0038) | 0.033 (0.017) |
| Benzaldehyde | 106.042 | $C_7H_6O$ | 24 | 0.22 (0.043) | 0.084 (0.026) | 0.32 (0.13) |
| $C_8$ Aromatics | 106.078 | $C_8H_{10}$ | 24 | 0.53 (0.17) | 0.21 (0.08) | 0.79 (0.37) |
| *(m,p)-Xylene*[d] | 106.078 | $C_8H_{10}$ | 15 | 0.16 (0.077) | 0.065 (0.033) | - |
| *Ethylbenzene*[d] | 106.078 | $C_8H_{10}$ | 15 | 0.12 (0.046) | 0.05 (0.022) | - |
| *o-Xylene*[d] | 106.078 | $C_8H_{10}$ | 15 | 0.062 (0.028) | 0.025 (0.012) | - |
| Quinone (=p-Benzoquinone) | 108.021 | $C_6H_4O_2$ | 24 | 0.20 (0.049) | 0.077 (0.02) | 0.30 (0.11) |
| 2-Methylphenol (=o-cresol), Anisol | 108.058 | $C_7H_8O$ | 24 | 0.57 (0.25) | 0.23 (0.11) | 0.87 (0.49) |
| 5-Methylfurfural, Benzene diols (=catechol, resorcinol) | 110.037 | $C_6H_6O_2$ | 24 | 0.62 (0.24) | 0.25 (0.12) | 0.96 (0.52) |
| $C_3$ Furans | 110.073 | $C_7H_{10}O$ | 24 | 0.11 (0.052) | 0.046 (0.024) | 0.18 (0.10) |
| Dihydroxy pyridine, Methyl maleimide | 111.032 | $C_5H_5NO_2$ | 24 | 0.06 (0.017) | 0.024 (0.0084) | 0.092 (0.04) |
| Chlorobenzene[d] | 112.008 | $C_6H_5Cl$ | 14 | 4.5e-04 (2.4e-04) | 2e-04 (1.3e-04) | 7.5e-04 (5.2e-04) |
| 5-Hydroxy-2-furfural/2-furoic acid | 112.016 | $C_5H_4O_3$ | 24 | 0.32 (0.07) | 0.12 (0.031) | 0.48 (0.17) |
| 2-Hydroxy-3-methyl-2-cyclopenten-1-one | 112.052 | $C_6H_8O_2$ | 24 | 0.29 (0.13) | 0.12 (0.061) | 0.46 (0.26) |
| Ethylcyclopentanone | 112.089 | $C_7H_{12}O$ | 24 | 0.034 (0.016) | 0.014 (0.007) | 0.053 (0.03) |
| Nitrofuran | 113.011 | $C_4H_3NO_3$ | 24 | 0.013 (0.0044) | 0.0051 (0.0019) | 0.019 (0.0088) |
| 5-hydroxymethyl-2[3H]-furanone | 114.032 | $C_5H_6O_3$ | 24 | 0.063 (0.024) | 0.026 (0.011) | 0.098 (0.049) |
| $C_6$ 1-DBE esters, $C_6$ Diones | 114.068 | $C_6H_{10}O_2$ | 24 | 0.093 (0.032) | 0.039 (0.017) | 0.15 (0.076) |
| Heptanal, 2,4-Dimethyl-3-pentanone, Heptanone | 114.104 | $C_7H_{14}O$ | 24 | 0.017 (0.0048) | 0.0072 (0.0025) | 0.027 (0.012) |
| 2,2,4-Trimethylpentane[e] | 114.141 | $C_8H_{18}$ | 13 | 0.071 (0.046) | 0.028 (0.018) | 0.11 (0.073) |
| n-Octane[e] | 114.141 | $C_8H_{18}$ | 15 | 0.052 (0.038) | 0.021 (0.017) | 0.082 (0.07) |
| 2-Methylheptane[e] | 114.141 | $C_8H_{18}$ | 14 | 0.034 (0.11) | 0.015 (0.048) | 0.056 (0.18) |
| 2,3,4-Trimethylpentane[e] | 114.141 | $C_8H_{18}$ | 3 | 0.015 (0.021) | 0.0067 (0.01) | 0.026 (0.04) |
| 3-Methylheptane[e] | 114.141 | $C_8H_{18}$ | 6 | 0.017 (0.022) | 0.0074 (0.01) | 0.028 (0.04) |
| 5-hydroxymethyl tetrahydro 2-furanone, 5-hydroxy tetrahydro 2-furfural | 116.047 | $C_5H_8O_3$ | 24 | 0.08 (0.038) | 0.034 (0.019) | 0.13 (0.08) |
| $C_6$ Esters | 116.084 | $C_6H_{12}O_2$ | 24 | 0.028 (0.015) | 0.011 (0.0062) | 0.044 (0.026) |
| Benzeneacetonitrile | 117.058 | $C_8H_7N$ | 24 | 0.023 (0.0071) | 0.0096 (0.0034) | 0.037 (0.016) |
| Chloroform[d] | 117.914 | $CHCl_3$ | 7 | 7.5e-04 (5.9e-04) | 3.6e-04 (2.9e-04) | 0.0014 (0.0012) |
| Benzofuran | 118.042 | $C_8H_6O$ | 24 | 0.096 (0.028) | 0.041 (0.015) | 0.16 (0.072) |
| Methylstyrenes, Indane, Propenylbenzenes | 118.078 | $C_9H_{10}$ | 24 | 0.086 (0.041) | 0.037 (0.019) | 0.14 (0.081) |
| Isobutyl nitrate, 2-butyl nitrate[d] | 119.058 | $C_4H_9NO_3$ | 7 | 0.0047 (0.0029) | 0.0019 (0.0011) | 0.0073 (0.0048) |
| Tolualdehydes | 120.058 | $C_8H_8O$ | 24 | 0.19 (0.053) | 0.082 (0.03) | 0.31 (0.14) |
| $C_9$ Aromatics | 120.094 | $C_9H_{12}$ | 24 | 0.16 (0.064) | 0.069 (0.031) | 0.26 (0.14) |

| | | | | | | |
|---|---|---|---|---|---|---|
| *1,2,3-Trimethylbenzene*[e] | 120.094 | $C_9H_{12}$ | 16 | 0.19 (0.23) | 0.089 (0.11) | - |
| *1,2,4-Trimethylbenzene*[e] | 120.094 | $C_9H_{12}$ | 15 | 0.17 (0.21) | 0.076 (0.099) | - |
| *4-Ethyltoluene*[e] | 120.094 | $C_9H_{12}$ | 14 | 0.10 (0.15) | 0.045 (0.071) | - |
| *3-Ethyltoluene*[e] | 120.094 | $C_9H_{12}$ | 14 | 0.079 (0.098) | 0.034 (0.046) | - |
| *2-Ethyltoluene*[e] | 120.094 | $C_9H_{12}$ | 14 | 0.058 (0.11) | 0.025 (0.051) | - |
| *Isopropylbenzene*[e] | 120.094 | $C_9H_{12}$ | 13 | 0.03 (0.054) | 0.013 (0.025) | - |
| *n-Propylbenzene*[e] | 120.094 | $C_9H_{12}$ | 12 | 0.015 (0.0084) | 0.0064 (0.0039) | - |
| *1,3,5-Trimethylbenzene*[e] | 120.094 | $C_9H_{12}$ | 7 | 0.0085 (0.0069) | 0.0036 (0.0027) | - |
| 2-Hydroxybenzaldehyde (=Salicylaldehyde) | 122.037 | $C_7H_6O_2$ | 24 | 0.15 (0.041) | 0.065 (0.023) | 0.25 (0.11) |
| $C_2$ Phenols, Methyl anisol | 122.073 | $C_8H_{10}O$ | 24 | 0.22 (0.11) | 0.10 (0.057) | 0.39 (0.24) |
| Hydroxybenzoquinone | 124.016 | $C_6H_4O_3$ | 24 | 0.098 (0.052) | 0.045 (0.026) | 0.17 (0.11) |
| Guaiacol (=2-methoxyphenol) | 124.052 | $C_7H_8O_2$ | 24 | 0.58 (0.32) | 0.27 (0.17) | 1.00 (0.70) |
| 5-(Hydroxymethyl)-2-furfural | 126.032 | $C_6H_6O_3$ | 24 | 0.14 (0.047) | 0.064 (0.026) | 0.24 (0.12) |
| n-Nonane[e] | 128.156 | $C_9H_{20}$ | 15 | 0.033 (0.024) | 0.015 (0.012) | 0.058 (0.048) |
| 1,1,1-Trichloroethane[d] | 131.93 | $C_2H_3Cl_3$ | 12 | 4.3e-04 (6.5e-04) | 2.1e-04 (3.2e-04) | 8.2e-04 (0.0012) |
| Methylbenzofurans | 132.058 | $C_9H_8O$ | 24 | 0.094 (0.036) | 0.046 (0.021) | 0.17 (0.092) |
| Ethyl styrenes, Methylpropenylbenzenes, Butenylbenzenes | 132.094 | $C_{10}H_{12}$ | 24 | 0.083 (0.053) | 0.04 (0.026) | 0.15 (0.11) |
| 3-Methylacetophenone | 134.073 | $C_9H_{10}O$ | 24 | 0.092 (0.034) | 0.045 (0.019) | 0.17 (0.086) |
| $C_{10}$ Aromatics | 134.11 | $C_{10}H_{14}$ | 24 | 0.081 (0.039) | 0.04 (0.021) | 0.15 (0.09) |
| Methylbenzoic acid | 136.052 | $C_8H_8O_2$ | 24 | 0.13 (0.047) | 0.066 (0.029) | 0.25 (0.13) |
| Monoterpenes | 136.125 | $C_{10}H_{16}$ | 24 | 0.41 (0.30) | 0.21 (0.15) | 0.79 (0.61) |
| *Camphene*[d] | 136.125 | $C_{10}H_{16}$ | 15 | 0.03 (0.021) | 0.016 (0.011) | - |
| *a-Pinene*[d] | 136.125 | $C_{10}H_{16}$ | 15 | 0.026 (0.02) | 0.014 (0.012) | - |
| *b-Pinene, Myrcene*[d] | 136.125 | $C_{10}H_{16}$ | 10 | 0.021 (0.014) | 0.011 (0.0079) | - |
| *Tricyclene*[d] | 136.125 | $C_{10}H_{16}$ | 15 | 0.0047 (0.0032) | 0.0025 (0.0018) | - |
| Nitrotoluene | 137.048 | $C_7H_7NO_2$ | 23 | 0.014 (0.0057) | 0.0071 (0.0034) | 0.027 (0.015) |
| 2-Methoxy-4-methylphenol (= creosol) | 138.068 | $C_8H_{10}O_2$ | 24 | 0.27 (0.18) | 0.14 (0.11) | 0.54 (0.44) |
| Methyl iodide[d] | 141.928 | $CH_3I$ | 15 | 0.0014 (7e-04) | 7.7e-04 (5.2e-04) | 0.0029 (0.0022) |
| Methylnaphthalene | 142.078 | $C_{11}H_{10}$ | 24 | 0.096 (0.041) | 0.05 (0.024) | 0.19 (0.10) |
| Product of levoglucosan dehydration (pyrolysis) | 144.042 | $C_6H_8O_4$ | 24 | 0.078 (0.052) | 0.042 (0.03) | 0.16 (0.12) |
| Dimethylbenzofuran | 146.073 | $C_{10}H_{10}O$ | 24 | 0.095 (0.047) | 0.051 (0.028) | 0.20 (0.12) |
| Methyl chavicol (estragole) | 148.089 | $C_{10}H_{12}O$ | 24 | 0.046 (0.026) | 0.025 (0.015) | 0.097 (0.062) |
| $C_{11}$ Aromatics | 148.125 | $C_{11}H_{16}$ | 24 | 0.025 (0.013) | 0.014 (0.0074) | 0.052 (0.031) |
| Vinyl guaiacol | 150.068 | $C_9H_{10}O_2$ | 24 | 0.063 (0.041) | 0.036 (0.025) | 0.14 (0.10) |
| Vanillin | 152.047 | $C_8H_8O_3$ | 18 | 0.04 (0.041) | 0.022 (0.023) | 0.083 (0.092) |
| Oxygenated monoterpenes, Camphor | 152.12 | $C_{10}H_{16}O$ | 24 | 0.045 (0.027) | 0.025 (0.014) | 0.094 (0.059) |
| Syringol | 154.063 | $C_8H_{10}O_3$ | 24 | 0.03 (0.011) | 0.017 (0.0067) | 0.065 (0.031) |
| Cineole, Other oxygenated monoterpenes | 154.136 | $C_{10}H_{18}O$ | 24 | 0.0048 (0.0029) | 0.0027 (0.0017) | 0.01 (0.0071) |
| 1,3-Dimethylnaphthalene | 156.094 | $C_{12}H_{12}$ | 24 | 0.051 (0.027) | 0.03 (0.018) | 0.12 (0.074) |
| Decanal | 156.151 | $C_{10}H_{20}O$ | 21 | 0.0067 (0.0031) | 0.0037 (0.0017) | 0.014 (0.0076) |

| | | | | | | |
|---|---|---|---|---|---|---|
| $C_{12}$ Aromatics | 162.141 | $C_{12}H_{18}$ | 24 | 0.01 (0.0061) | 0.0062 (0.0036) | 0.024 (0.015) |
| Eugenol + isoeugenol | 164.084 | $C_{10}H_{12}O_2$ | 24 | 0.032 (0.021) | 0.02 (0.014) | 0.076 (0.058) |
| $C_{13}$ Aromatics | 176.156 | $C_{13}H_{20}$ | 24 | 0.013 (0.0065) | 0.0085 (0.0047) | 0.033 (0.02) |
| Sesquiterpenes | 204.188 | $C_{15}H_{24}$ | 23 | 0.038 (0.038) | 0.029 (0.028) | 0.11 (0.11) |
| *Black carbon*[g] | - | - | 24 | 4.95 (2.00)[i] | 0.389 (0.17) | - |
| *Organic carbon*[h] | - | - | 24 | 145.00 (23.00)[i] | 11.60 (3.30) | - |
| **Total VOC emissions** | | | | **148.26 (29.61)** | **26.11 (6.92)** | |

*Note.* Uncertainties are reported as the standard deviation (1σ) of the campaign average, representing fire-to-fire variability. The corresponding campaign average MCE is 0.90. [a]VOC contributors to PTR-ToF-MS measured ion masses are assigned based on Koss et al. (2018) and listed in order of most abundant isomeric contribution. Italicized VOC contributors are shown for speciation purposes but not included in the total carbon term of the carbon mass balance nor total emissions calculations (Section 2.4). [b]Dominant/Primary isotopologue exact mass. [c]Number of emission transects sampled more than 30 minutes apart. [d]Trace organic gas analyzer (TOGA). [e]Advanced whole air sampler (AWAS). [f]Iodide-adduct time-of-flight chemical-ionization mass ($I^-$ CIMS). [g]Single particle soot photometer (SP2). [h]High-resolution aerosol mass spectrometer (HR-AMS). [i]μg $sm^{-3}$ $ppm^{-1}$ CO.